Graphical Abstract

Delamination of a sandwich layer by diffusion of a corrosive species: initiation of growth

Alessandro Leronni, Norman A. Fleck

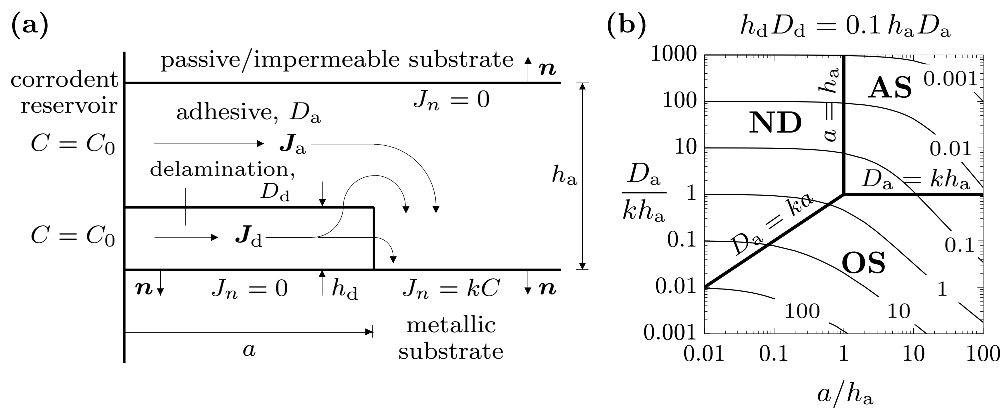

(a) Diffusion of a corrodent towards a delamination tip in a sandwich layer

(b) Diffusion maps for the steady-state tip flux $J_{\mathrm{tip}} = kC_{\mathrm{tip}}$, dictating the initiation time for delamination, with regimes of behaviour highlighted (ND: negligible delamination, AS: adhesive strip, OS: outer singularity)

Highlights

Delamination of a sandwich layer by diffusion of a corrosive species: initiation of growth

Alessandro Leronni, Norman A. Fleck

- Singularity analysis of diffusion to a delamination tip along two paths
- A diffusion map for the flux of a corrosive species to a delamination tip
- Prediction of initiation time for delamination in a sandwich layer

Delamination of a sandwich layer by diffusion of a corrosive species: initiation of growth

Alessandro Leronni, Norman A. Fleck*

Cambridge University Engineering Department,
Trumpington Street, Cambridge, CB2 1PZ, UK

Abstract

A fundamental study is reported on the initiation of crack growth from a pre-existing delamination; growth is due to the diffusion of a corrosive species from the side face of a sandwich layer. The corrodent diffuses along the delamination and simultaneously through the sandwich layer. It is envisaged that a chemical reaction occurs on the intact interface ahead of the delamination tip, at a rate that scales with the local concentration of corrodent. Debonding initiates at the tip of the pre-existing delamination when a critical quantity of corrodent per unit area has reacted at the interface immediately ahead of the tip. Diffusion theory is used to predict the duration of the initial transient prior to the establishment of a steady-state value of reaction rate at the interface, directly ahead of the delamination. Once steady state has been attained, the Laplace equation is solved for the corrodent concentration within the sandwich layer and delamination zone. The reaction rate at the delamination tip and the time to initiate debonding of the interface

*Corresponding author

Email addresses: al2040@cam.ac.uk (Alessandro Leronni), naf1@cam.ac.uk (Norman A. Fleck)

Preprint submitted to Journal of the Mechanics and Physics of Solids December 17, 2021

are determined. Maps are constructed to show regimes of behaviour, with axes that make use of the sandwich layer geometry and the relative diffusivity of corrodent within the delamination crack and within the sandwich layer. A number of asymptotic solutions shed light on the general numerical case. The analysis is motivated by the practical problem of delamination of adhesive joints employed in ship construction, but has much wider applicability.
Keywords:
adhesion and adhesives, corrosion and embrittlement, delamination, diffusion, fracture

---

1. Introduction

Progressive interfacial delamination by the chemical attack of a diffusing species is a ubiquitous failure mechanism across a wide range of engineering fields. For example, steel reinforcement bars in reinforced concrete structures rust and debond (Poursaee, 2016), glass fibre reinforced epoxy composites degrade when immersed in oxygenated sea-water (Merah et al., 2010) and adhesive joints delaminate in an aggressive environment (Gettings et al., 1977; Kinloch, 1979; Bordes et al., 2009).

Consider the debonding of a pre-cracked adhesive/steel joint immersed in oxygenated water by *free corrosion*. The prototypical problem is sketched in Fig. 1(a). Oxygen and water diffuse through the adhesive from a side face to the adhesive/steel interface. Suppose that the pre-existing delamination is water-filled by capillarity and acts as an additional path for oxygen diffusion (Leng et al., 1998a; Bordes et al., 2009; Fleck and Willis, 2021). Iron (Fe) of the steel substrate reacts with water (H_2O) and oxygen (O_2) dissolved within

(a)

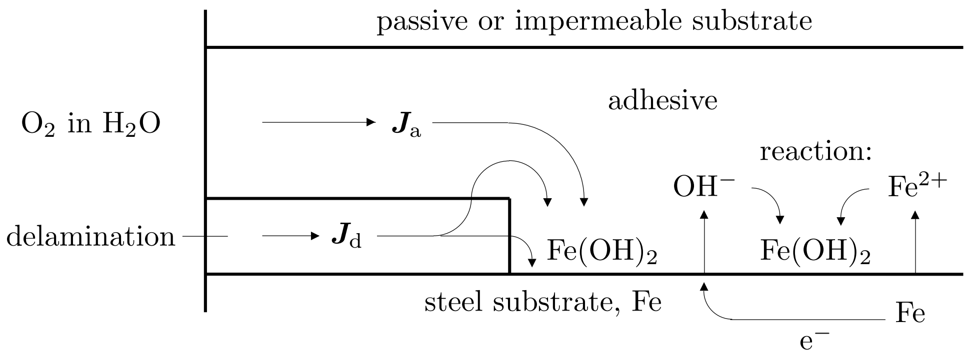

(b)

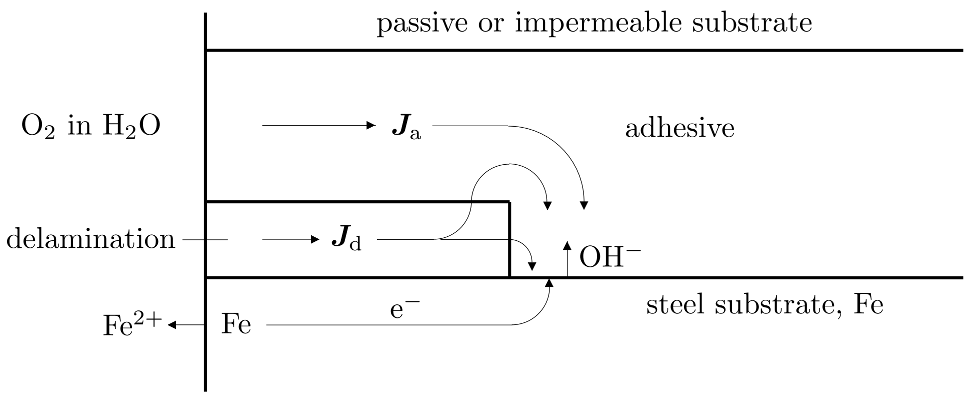

Figure 1: **(a)** Free corrosion and **(b)** cathodic delamination. $\boldsymbol{J}_a$ and $\boldsymbol{J}_d$ denote the flux of O_2 within the adhesive and delamination, respectively.

the adhesive to produce rust in the form of ferrous hydroxide ($Fe(OH)_2$) such that

$$2Fe + 2H_2O + O_2 \rightarrow 2Fe(OH)_2 \quad (1)$$

The full reaction (1) comprises two half-reactions as sketched in Fig. 1(a). Small regions of the steel surface undergo an anodic half-reaction

$$2Fe \rightarrow 2Fe^{2+} + 4e^{-} \quad (2)$$

The Fe^{2+} ions are liberated from the surface of the steel, while the electrons flow through the steel to adjacent surface regions that behave in a cathodic manner such that

$$2H_2O + O_2 + 4e^{-} \rightarrow 4OH^{-} \quad (3)$$

The Fe^{2+} and OH^{-} react to form rust $Fe(OH)_2$ and this leads to delamination of the interface. Typically, oxygen diffusion through the adhesive and along the pre-existing delamination is rate-limiting for the reaction (1). Therefore, it suffices to consider the diffusion of oxygen alone.

An alternative corrosion mechanism is *cathodic delamination* (Leidheiser, 1987; Stratmann et al., 1994; Leng et al., 1998b), see Fig. 1(b). The same half-reactions (2) and (3) occur as in free corrosion, but now the anodic region of Fe^{2+} production is remote from the cathodic region of OH^{-} production. Consequently, the $Fe(OH)_2$ forms in the remote reservoir where the Fe^{2+} is produced. Assume that interfacial debonding is by OH^{-} attack of the interface at the tip of the pre-existing delamination; the rate of production of OH^{-} scales with the flux of oxygen to the interface. To maintain electroneutrality within the electrolyte-filled delamination it is necessary for cations, such as Na^{+} in the case of sea-water, to electro-diffuse along the delamination.

However, if the concentration and mobility of cations are sufficiently high, the kinetics of OH^- production at the delamination tip are again dictated by oxygen supply.

There exist other possible corrosion mechanisms that simply involve the transport of water alone to the adhesive/steel interface. For example, the interfacial bond between adhesive and steel substrate can be weakened by hydration. Or, a reverse condensation reaction (*hydrolysis*) can occur in the adhesive, such that water leads to chain breakage and is thereby consumed (Gledhill and Kinloch, 1974; Schmidt and Bell, 1986).

Regardless of the specific mechanism, it is assumed in the present study that the onset of delamination growth is dictated by the flux of a single corrosive species, hereafter termed corrodent, to the intact adhesive/steel interface. Henceforth, refer to the time for the initiation of delamination growth as the delamination time. If the delamination time much exceeds the time required to establish a steady-state flux of corrodent to the delamination tip, then it is only necessary to consider the steady-state diffusion of corrodent in the adhesive and in the delamination zone. The rigorous mathematical treatment of this problem is presented in the following, and builds upon the recent study of Fleck and Willis (2021); they addressed the steady-state advance of a delamination rather than its initiation. Specifically, Fleck and Willis (2021) obtained the delamination velocity of a semi-infinite interfacial crack, with the concentration of corrodent prescribed along the delamination.

2. Problem statement

With reference to Fig. 2, idealise a pre-cracked adhesive joint by an adhesive sandwich layer of height h_a containing a delamination of length a and uniform height h_d, with $h_\mathrm{d} \ll h_\mathrm{a}$. The pre-crack may represent a manufacturing defect, such as poor adhesion. The adhesive layer is semi-infinite in length and its left-hand face is in contact with an infinite reservoir of a corrodent that can diffuse through the adhesive and along the delamination. Upon reaching the adhesive/metal interface, the corrodent reacts with the interface and ultimately debonds it.

Write C as the molar concentration of corrodent and $\boldsymbol{J}$ as its flux. Introduce a Cartesian reference frame (x, y) with origin at the pre-existing

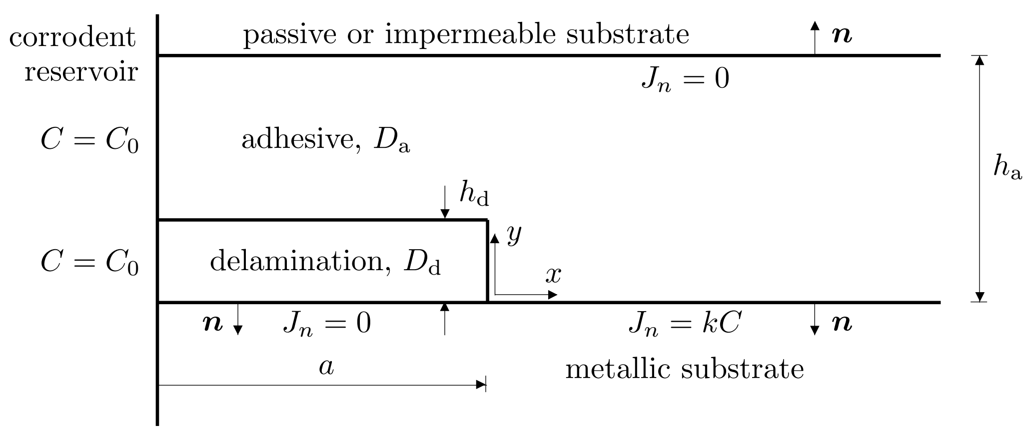

Figure 2: Delamination of an adhesive/metal joint by diffusion of a corrosive species: geometry, material parameters and boundary conditions.

delamination tip, as shown in Fig. 2. Mass conservation requires

$$\frac{\partial C}{\partial t} + \boldsymbol{\nabla} \cdot \boldsymbol{J} = 0 \tag{4}$$

where t denotes time and $\boldsymbol{\nabla}\cdot$ is the divergence operator. Assume that Fick's law holds and write D_{a} and D_{d} as the diffusion coefficients of the corrodent in the adhesive and delamination, respectively. Then,

$$\boldsymbol{J} = -D_{\mathrm{i}} \boldsymbol{\nabla} C \tag{5}$$

with $\mathrm{i} = \mathrm{a}$ in the adhesive and $\mathrm{i} = \mathrm{d}$ in the delamination; $\boldsymbol{\nabla}$ is the usual gradient operator. Substitution of (5) into (4) gives

$$\frac{\partial C}{\partial t} = D_{\mathrm{i}} \nabla^2 C \tag{6}$$

in terms of the usual Laplacian ∇^2.

The outward flux of corrodent from the adhesive or delamination into the interface with the metal substrate is $J_n = \boldsymbol{J} \cdot \boldsymbol{n}$, where $\boldsymbol{n}$ is the unit outward normal, as defined in Fig. 2. Assume that the chemical reaction of corrodent is quantified by the flux J_n of corrodent into the adhesive/metal interface, such that

$$J_n = kC\,, \qquad x > 0\,,\; y = 0 \tag{7}$$

where the mass transfer coefficient k is the relevant rate constant of the reaction, and is taken to be independent of C. The delamination/metal interface is insulating such that

$$J_n = 0\,, \qquad x < 0\,,\; y = 0 \tag{8}$$

consistent with the notion of a passivated state behind the delamination tip. The left-hand side of the joint is in contact with an infinite reservoir of corrodent; hence

$$C = C_0\,, \qquad x = -a\,,\, 0 < y < h_{\mathrm{a}} \tag{9}$$

where C_0 takes, as an upper limit, the saturation concentration in the adhesive. The flux J_n vanishes along the top face of the adhesive when the uppermost layer is impermeable, such as a composite of negligible permeability. Alternatively, the top face can be regarded as a symmetry plane for a metal/adhesive/metal sandwich structure with an adhesive layer of height $2h_{\mathrm{a}}$. Both C and J_n are continuous across the ideal interface between delamination and adhesive. Initially, the concentration C within the adhesive layer and delamination vanishes, $C(x, y, t = 0) = 0$.

An initial transient of duration t_{I} exists over which the governing partial differential equation (6) holds. During this transient, the tip flux $J_n(x = 0^+, y = 0, t)$ gradually increases from zero to the steady-state value J_{tip}. After steady state has been attained, (6) reduces to the much simpler Laplace equation

$$\nabla^2 C = 0 \tag{10}$$

The relation $J_{\mathrm{tip}} = kC_{\mathrm{tip}}$ holds on the basis of (7). For definiteness, assume that the initial transient phase ends at a time t_{I} such that

$$J_n(x = 0^+, y = 0, t = t_{\mathrm{I}}) = 0.9\, J_{\mathrm{tip}} \tag{11}$$

where the factor of 0.9 is arbitrary. Over the initial transient, the total amount of reacted corrodent per unit area along the adhesive/metal interface is

$$Q_{\mathrm{I}} = \int_0^{t_{\mathrm{I}}} J_n(t')\,\mathrm{d}t' = k \int_0^{t_{\mathrm{I}}} C(t')\,\mathrm{d}t'\,, \qquad x > 0\,,\, y = 0 \tag{12}$$

upon recalling (7). The total amount of reacted corrodent per unit area at the delamination tip at time $t > t_\mathrm{I}$ can be written as

$$Q(t) = Q_\mathrm{I} + J_\mathrm{tip}(t - t_\mathrm{I}) \,, \qquad t > t_\mathrm{I} \quad \text{and} \quad x = 0^+ \,, \, y = 0 \qquad (13)$$

Now assume that debonding initiates when the value of Q at the pre-existing delamination tip reaches a critical value Q^*, where Q^* can be interpreted as a measure of the resistance of the adhesive/metal interface to debonding. The delamination time t^* is such that

$$Q(x = 0^+, y = 0, t = t^*) = Q^* \qquad (14)$$

For the case where $Q^* > Q_\mathrm{I}$, t^* can be written as

$$t^* = \frac{Q^* - Q_\mathrm{I}}{J_\mathrm{tip}} + t_\mathrm{I} \qquad (15)$$

via (13) and (14). Further, if $t^* \gg t_\mathrm{I}$, (15) reduces to

$$t^* \approx \frac{Q^*}{J_\mathrm{tip}} \qquad (16)$$

Equation (15) reveals that, if $t^* \gg t_\mathrm{I}$, the problem of obtaining t^* reduces to that of finding J_tip, requiring only the solution of the Laplace equation (10). This is the main focus of the present investigation; the steady-state numerical solution is presented and a number of asymptotic solutions are derived to show the regimes of behaviour. For completeness, the time-dependent diffusion equation (6) is also solved numerically, and the relevance of the steady-state solution is thereby assessed.

3. Nondimensionalisation

The diffusion equation (6) along with the boundary and initial conditions suggest that the concentration $C(x, y, t)$ can be written in terms of the following non-dimensional independent groups:

$$\frac{C}{C_0} = f\left(\frac{x}{h_\mathrm{a}}, \frac{y}{h_\mathrm{a}}, \frac{D_\mathrm{a}t}{h_\mathrm{a}^2}, \frac{a}{h_\mathrm{a}}, \frac{l}{h_\mathrm{a}}, \frac{h_\mathrm{d}}{h_\mathrm{a}}, \frac{D_\mathrm{d}}{D_\mathrm{a}}\right) \tag{17}$$

where, for later convenience, a material length scale

$$l \equiv \frac{D_\mathrm{a}}{k} \tag{18}$$

has been introduced. The Biot number

$$\mathrm{Bi} \equiv \frac{kh_\mathrm{a}}{D_\mathrm{a}} = \frac{h_\mathrm{a}}{l} \tag{19}$$

follows immediately.

Given that $h_\mathrm{d} \ll h_\mathrm{a}$ and $D_\mathrm{d} \gg D_\mathrm{a}$, it is expected that the combined non-dimensional group $(h_\mathrm{d}D_\mathrm{d})/(h_\mathrm{a}D_\mathrm{a})$ plays a major role instead of the two groups $h_\mathrm{d}/h_\mathrm{a}$ and $D_\mathrm{d}/D_\mathrm{a}$. The case where the individual values of $h_\mathrm{d}/h_\mathrm{a}$ and $D_\mathrm{d}/D_\mathrm{a}$ each play a role is analysed subsequently in Sec. 5. The combined group $(h_\mathrm{d}D_\mathrm{d})/(h_\mathrm{a}D_\mathrm{a})$ expresses the ratio of a "current" diffusing per unit time across the delamination cross-section h_d relative to that across the adhesive cross-section h_a. When this idealisation is valid, (17) can be slightly simplified to

$$\frac{C}{C_0} = f\left(\frac{x}{h_\mathrm{a}}, \frac{y}{h_\mathrm{a}}, \frac{D_\mathrm{a}t}{h_\mathrm{a}^2}, \frac{a}{h_\mathrm{a}}, \frac{l}{h_\mathrm{a}}, \frac{h_\mathrm{d}D_\mathrm{d}}{h_\mathrm{a}D_\mathrm{a}}\right) \tag{20}$$

The steady-state corrodent flux into the adhesive/metal interface, directly ahead of the delamination tip, can be expressed in similar non-dimensional fashion as

$$\frac{J_\mathrm{tip}h_\mathrm{a}}{D_\mathrm{a}C_0} = f\left(\frac{a}{h_\mathrm{a}}, \frac{l}{h_\mathrm{a}}, \frac{h_\mathrm{d}D_\mathrm{d}}{h_\mathrm{a}D_\mathrm{a}}\right). \tag{21}$$

The nature of the functional relationship (21) is explored below, and the overall behaviour is summarised in the form of diffusion maps.

4. Regimes of behaviour

Contours of tip flux $J_{\rm tip}h_{\rm a}/(D_{\rm a}C_0)$ are plotted on a map with axes ($a/h_{\rm a}$, $l/h_{\rm a}$) for selected values of $(h_{\rm d}D_{\rm d})/(h_{\rm a}D_{\rm a}) = 0, 0.1, 1, 10$, see Fig. 3. The contours are derived by solving Laplace's equation (10) in both the adhesive and delamination regions, for the case of $h_{\rm d}$ much smaller than all other length scales entering the problem.[1]

Geometric transition values ($a = h_{\rm a}$, $l = h_{\rm a}$, $l = a$) are displayed on the maps and identify the boundaries between four distinct regimes of behaviour. The dominant diffusion mechanisms and associated distribution of flux along the adhesive/metal interface are sketched in Fig. 4 for each regime. Each regime is now introduced, with a full analysis given later.

(a) *Negligible delamination* (ND) regime, $a \ll (h_{\rm a}, l)$. The presence of the delamination layer has a negligible effect upon the tip flux, which simply reads $J_{\rm tip} \approx kC_0$. The data point (1) in Fig. 3(b) lies within this regime and the full numerical solution for this case is given in Fig. 4(a).

(b) *Adhesive strip* (AS) regime, $h_{\rm a} \ll (a, l)$. The adhesive layer behaves as a thin strip, and the corrodent migrates into the interface over a length λ ahead of the delamination tip, where $h_{\rm a} \ll \lambda \ll l$. Diffusion in the adhesive strip is treated as one-dimensional, depending only upon the co-ordinate x. The data point (2) in Fig. 3(b) is representative of this regime, and the numerical solution for this point (2) is given in Fig. 4(b).

[1]The finite element software COMSOL Multiphysics, version 5.6, is used to solve for a large number of cases and then MATLAB, version R2020A, is used to interpolate the data and construct the contours.

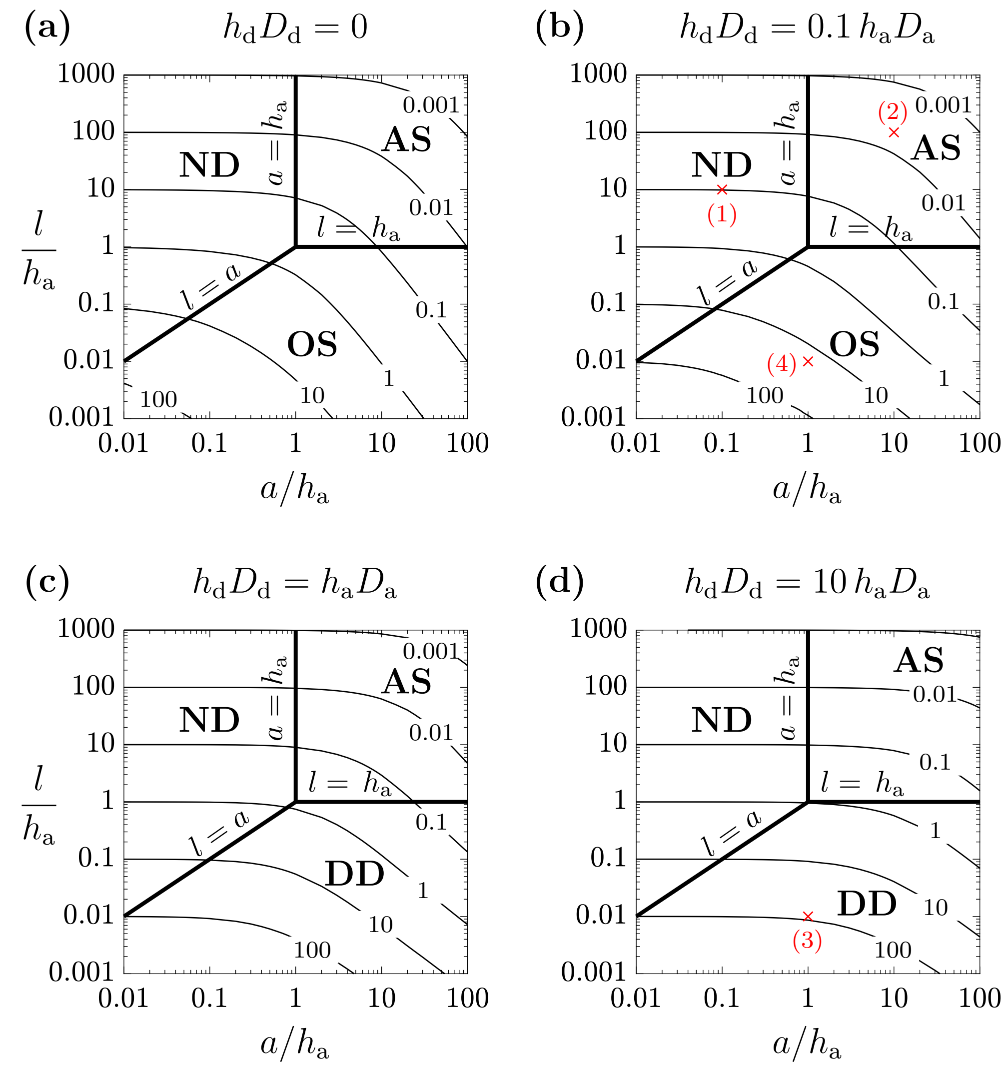

Figure 3: Contour plots of $J_\mathrm{tip}h_\mathrm{a}/(D_\mathrm{a}C_0)$ on a map with axes (a/h_a, l/h_a), for $(h_\mathrm{d}D_\mathrm{d})/(h_\mathrm{a}D_\mathrm{a})$ equal to **(a)** 0, **(b)** 0.1, **(c)** 1 and **(d)** 10. The dominant regimes of behaviour are indicated: ND (negligible delamination), AS (adhesive strip), DD (dominant delamination) and OS (outer singularity). The four data points × shown in Figs. 3(b) and (d) denote representative solutions that are detailed in Fig. 4.

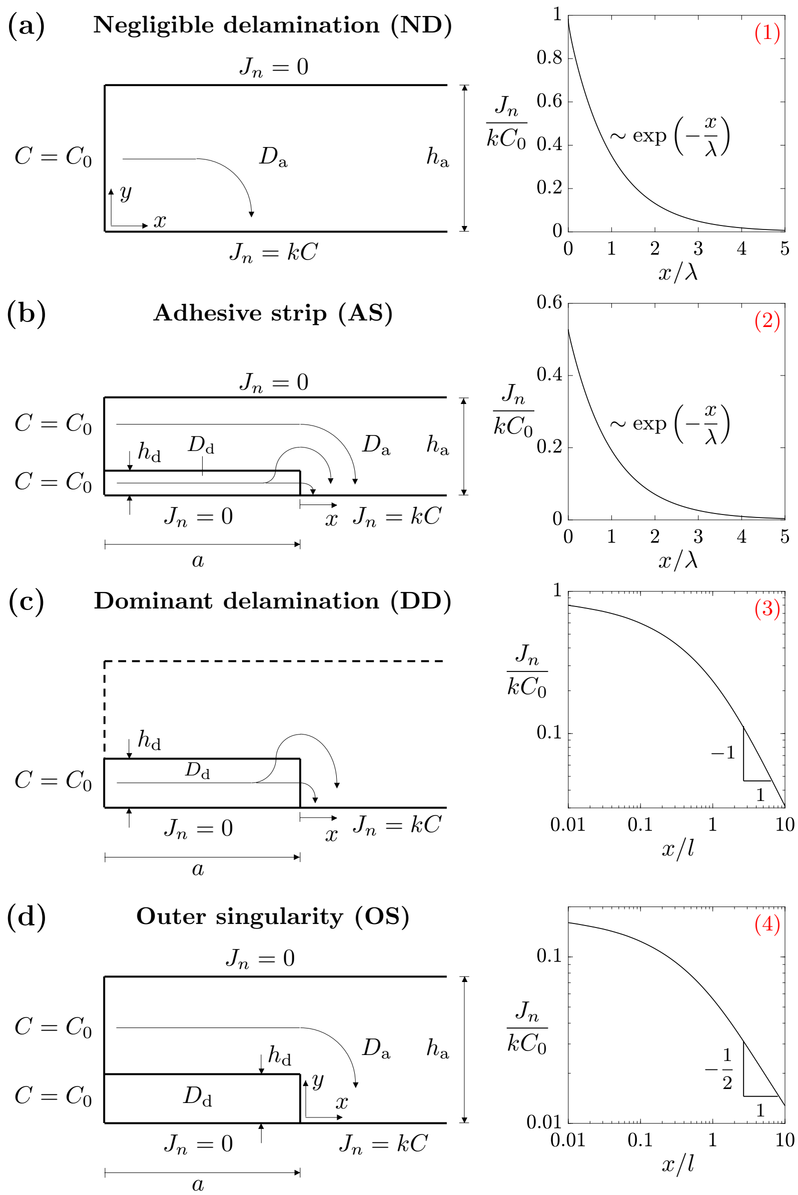

Figure 4: Regimes of behaviour: **(a)** Negligible delamination (ND), **(b)** adhesive strip (AS), **(c)** dominant delamination (DD), and **(d)** outer singularity (OS). For each regime, a sketch of the diffusion mechanism and the plot of $J_n/(kC_0)$ versus x for the data points (1) to (4) indicated in Figs. 3(b) and (d) are given.

(c) *Dominant delamination* (DD) regime, $h_\mathrm{d}D_\mathrm{d} \gg h_\mathrm{a}D_\mathrm{a}$ and $l \ll (a, h_\mathrm{a})$. The current of corrodent flowing in the delamination zone dominates that in the adhesive layer, and corrodent reacts at the interface over a length on the order of l from the delamination tip. Point (3) on Fig. 3(d) is representative of the DD regime, with numerical solution given in Fig. 4(c).

(d) *Outer singularity* (OS) regime, $h_\mathrm{d}D_\mathrm{d} \ll h_\mathrm{a}D_\mathrm{a}$ and $l \ll (a, h_\mathrm{a})$. In a finite annular zone surrounding the delamination tip there exists an outer singular field in the adhesive such that the flux scales as $r^{-1/2}$, where r is the radius from the delamination tip (in polar co-ordinates). The intensity of flux singularity is labelled as K, by analogy with the stress intensity factor K for a Mode III crack in linear elastic fracture mechanics (Anderson, 2017).

4.1. The "negligible delamination" regime

For the case $a = 0$, see Fig. 4(a), an analytical solution exists for the steady-state diffusion problem under investigation, given by the following infinite series:

$$\frac{C(x,y)}{C_0} = 2\mathrm{Bi}\sum_{n=1}^{\infty}\frac{\cos[\alpha_n(h_\mathrm{a}-y)]\exp(-\alpha_n x)}{(\mathrm{Bi}^2+\mathrm{Bi}+\alpha_n^2h_\mathrm{a}^2)\cos(\alpha_n h_\mathrm{a})} \tag{22}$$

where α_n are the positive roots of

$$\alpha_n h_\mathrm{a}\tan(\alpha_n h_\mathrm{a}) = \mathrm{Bi} \tag{23}$$

and the Biot number Bi has already been defined in (19). This solution is obtained by particularising the solution for heat flow in a finite rectangle as reported in Carslaw and Jaeger (1959) to the case of a semi-infinite rectangle. The interfacial flux is

$$J_n(x) = kC(x,0) = 2kC_0\mathrm{Bi}\sum_{n=1}^{\infty}\frac{\exp(-\alpha_n x)}{\mathrm{Bi}^2+\mathrm{Bi}+\alpha_n^2h_\mathrm{a}^2} \tag{24}$$

If Bi $\ll 1$, then $\alpha_1 h_\mathrm{a} \ll 1$, $\tan(\alpha_1 h_\mathrm{a}) \approx \alpha_1 h_\mathrm{a}$ and $\alpha_1 h_\mathrm{a} \approx \sqrt{\mathrm{Bi}}$, see (23). Upon considering only the leading term in the series, (24) simplifies to

$$J_n(x) \approx kC_0 \exp\left(-\frac{x}{\lambda}\right) \tag{25}$$

with $\lambda \equiv h_\mathrm{a}/\sqrt{\mathrm{Bi}} = \sqrt{h_\mathrm{a} l}$.

4.2. The "adhesive strip" regime

Now consider the case $h_\mathrm{a} \ll (a, l)$, as sketched in Fig. 4(b). A simple 1D solution for $C(x)$ in both the adhesive and delamination is adequate, as follows. Define the "current" $I_\mathrm{a}(x)$ in the adhesive as

$$I_\mathrm{a} = -h_\mathrm{a} D_\mathrm{a} \frac{\partial C}{\partial x} \tag{26}$$

Then, mass conservation in the adhesive implies, for $x > 0$:

$$\frac{\partial I_\mathrm{a}}{\partial x} = -kC \tag{27}$$

and substitution of (26) into (27) gives

$$\lambda^2 \frac{\partial^2 C}{\partial x^2} - C = 0 \tag{28}$$

where $\lambda = \sqrt{h_a l}$ as before. The solution is

$$C(x) = C_\mathrm{tip} \exp\left(-\frac{x}{\lambda}\right), \qquad x > 0 \tag{29}$$

where C_tip remains to be determined. The current I_a at $x = 0^+$ follows immediately from substitution of (29) into (26), to give

$$I_\mathrm{a}(x = 0^+) = \frac{h_\mathrm{a} D_\mathrm{a} C_\mathrm{tip}}{\lambda} \tag{30}$$

For $x < 0$, homogenise the adhesive and delamination into a single 1D strip of equivalent diffusivity D_{e}, such that

$$h_{\mathrm{a}} D_{\mathrm{e}} = h_{\mathrm{d}} D_{\mathrm{d}} + h_{\mathrm{a}} D_{\mathrm{a}} \tag{31}$$

upon making the usual assumption $h_{\mathrm{d}} \ll h_{\mathrm{a}}$. Then, since there is no corrodent leakage from the delamination into the substrate along $x < 0$, the current I_e in the effective medium is uniform for $x < 0$ and is of magnitude

$$I_e = h_{\mathrm{a}} D_{\mathrm{e}} (C_0 - C_{\mathrm{tip}})/a \,, \qquad x < 0 \tag{32}$$

By imposing continuity of current at $x = 0$, the relations (30) to (32) imply that

$$\frac{C_0}{C_{\mathrm{tip}}} = 1 + \left(1 + \frac{h_{\mathrm{d}} D_{\mathrm{d}}}{h_{\mathrm{a}} D_{\mathrm{a}}}\right)^{-1} \frac{a}{h_{\mathrm{a}}} \left(\frac{h_{\mathrm{a}}}{l}\right)^{1/2} \tag{33}$$

and $J_{\mathrm{tip}} = k C_{\mathrm{tip}}$ is given by

$$\frac{J_{\mathrm{tip}} h_{\mathrm{a}}}{D_{\mathrm{a}} C_0} = \frac{h_{\mathrm{a}}}{l} \left[1 + \left(1 + \frac{h_{\mathrm{d}} D_{\mathrm{d}}}{h_{\mathrm{a}} D_{\mathrm{a}}}\right)^{-1} \frac{a}{h_{\mathrm{a}}} \left(\frac{h_{\mathrm{a}}}{l}\right)^{1/2}\right]^{-1} \tag{34}$$

The full numerical solutions of Figs. 3(b) and (d) for $(h_{\mathrm{d}} D_{\mathrm{d}})/(h_{\mathrm{a}} D_{\mathrm{a}}) = 0.1$ and 10, respectively, are compared with the asymptotic solution (34). The comparison is done for l/h_{a} equal to 100 and 1000, by varying a/h_{a} between 1 and 100, for which the AS regime is operative. Fig. 5 shows that the simple estimate (34) adequately reproduces the full numerical solution.

4.3. The "dominant delamination" regime

Now consider the regime where the current of corrodent over the height h_{d} of the delamination, I_{d}, dominates the current over the height h_{a} of the adhesive. This occurs when $h_{\mathrm{d}} D_{\mathrm{d}} \gg h_{\mathrm{a}} D_{\mathrm{a}}$. Additionally, assume that

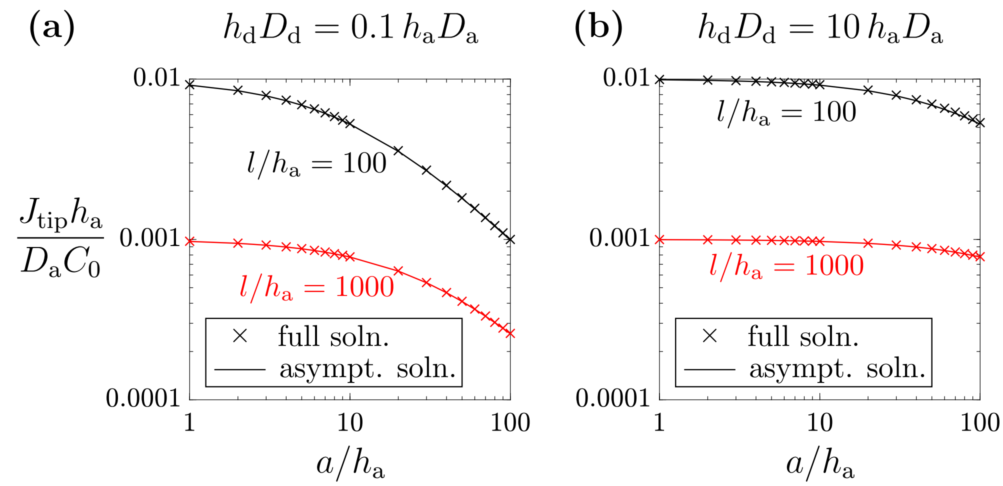

Figure 5: Adhesive strip (AS) regime. Comparison between full solution and asymptotic solution (34) for $(h_d D_d)/(h_a D_a)$ equal to **(a)** 0.1 and **(b)** 10, with l/h_a equal to 100 and 1000.

$(h_d, l) \ll (h_a, a)$. The DD regime is sketched in Fig. 4(c). Some side leakage from the delamination into the adhesive occurs in the vicinity of the delamination tip, $-(h_d, l) < x < 0$, but the high diffusivity within the delamination implies that the concentration is close to C_{tip} in this region. Sufficiently far behind the delamination tip, that is, for $x \ll -(h_d, l)$, the current I_d can be regarded as uniform along the delamination with negligible side leakage into the adhesive and consequently

$$I_d \approx h_d D_d (C_0 - C_{tip})/a \tag{35}$$

where C_{tip} remains to be determined.

The corrodent is extracted at a rate $J_n = kC$ along the adhesive/metal interface ahead of the delamination tip, and at a tip rate $J_{tip} = kC_{tip}$. The length scale $l = D_a/k$ can be interpreted as the length over which the interface reaction dominates diffusion within the adhesive, and consequently

$$J_{\mathrm{tip}} = \beta I_{\mathrm{d}}/l \tag{36}$$

where the parameter $\beta(h_{\mathrm{d}}/l)$ is on the order of unity. Full numerical simulations reveal that $J_{\mathrm{tip}}l/I_{\mathrm{d}} \approx 0.503 - 0.187\, h_{\mathrm{d}}/l$ for $h_{\mathrm{d}}/l < 0.1$, with the details omitted for the sake of brevity. Hence, for $h_{\mathrm{d}} \ll l$, (36) becomes

$$J_{\mathrm{tip}} \approx 0.503\, I_{\mathrm{d}}/l \tag{37}$$

Now eliminate I_{d} and C_{tip} from (35) and (37) and use the relation $J_{\mathrm{tip}} = kC_{\mathrm{tip}}$ to obtain

$$\frac{J_{\mathrm{tip}} h_{\mathrm{a}}}{D_{\mathrm{a}} C_0} = \frac{h_{\mathrm{a}}}{l}\left(1 + 1.988 \frac{a}{h_{\mathrm{a}}} \frac{h_{\mathrm{a}} D_{\mathrm{a}}}{h_{\mathrm{d}} D_{\mathrm{d}}}\right)^{-1} \tag{38}$$

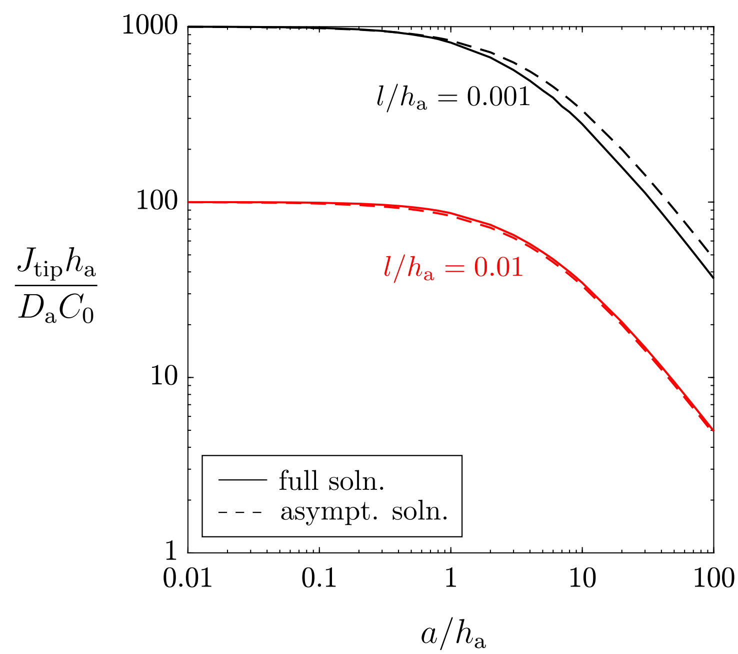

Figure 6: Dominant delamination (DD) regime. Comparison between full solution and asymptotic solution (38) for $h_{\mathrm{d}} D_{\mathrm{d}} = 10\, h_{\mathrm{a}} D_{\mathrm{a}}$, with l/h_{a} equal to 0.001 and 0.01.

Excellent agreement exists between the approximate solution (38) and the full numerical solution, see Fig. 6, for the choice $h_\mathrm{d} D_\mathrm{d} = 10\, h_\mathrm{a} D_\mathrm{a}$, and l/h_a equal to 0.001 and 0.01.

4.4. The "outer singularity" regime

Finally, consider the case where $(h_\mathrm{d}, l) \ll (h_\mathrm{a}, a)$, and also $h_\mathrm{d} D_\mathrm{d} \ll h_\mathrm{a} D_\mathrm{a}$. The steady-state distribution of non-dimensional flux along the intact adhesive/metal interface, $J_n h_\mathrm{a}/(D_\mathrm{a} C_0)$, is plotted as a function of x/h_d in Fig. 7, for selected values of h_d/l and $D_\mathrm{d}/D_\mathrm{a}$. Note that all responses converge to the same asymptotic solution over $(h_\mathrm{d}, l) \ll x \ll (h_\mathrm{a}, a)$.

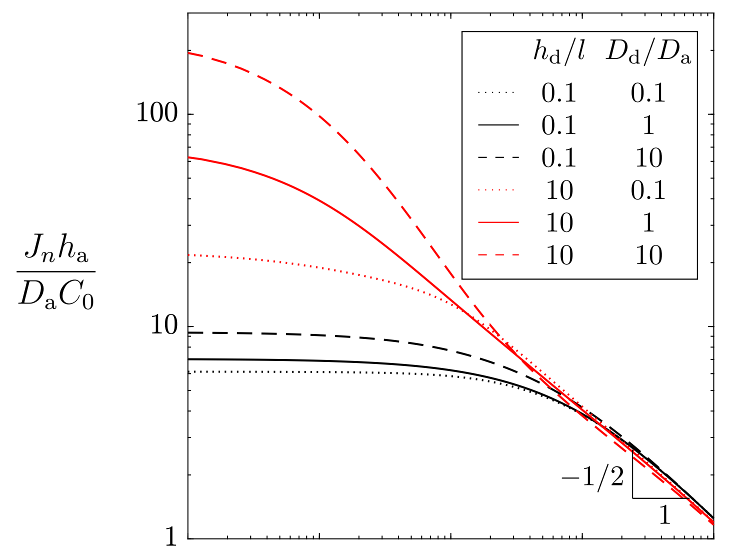

Figure 7: Distribution of interfacial flux ahead of delamination tip, for selected values of h_d/l and $D_\mathrm{d}/D_\mathrm{a}$, such that $(h_\mathrm{d}, l) \ll (h_\mathrm{a}, a)$ and $h_\mathrm{d} D_\mathrm{d} \ll h_\mathrm{a} D_\mathrm{a}$. All curves converge to the same asymptotic solution, of slope $-1/2$ on a log-log plot, for $(h_\mathrm{d}, l) \ll x \ll (h_\mathrm{a}, a)$. In all cases, $h_\mathrm{a} = a = 1000\, h_\mathrm{d}$.

It is straightforward to obtain the leading order term of this asymptotic solution by considering the case $l = 0$ and neglecting the presence of the thin delamination zone. Introduce polar co-ordinates (r, θ) centred on the delamination tip. The boundary condition along the adhesive/metal interface, equation (7), is replaced by $C(r, \theta = 0) = 0$, as sketched in Fig. 8. Assume that a separation-of-variables solution exists for $C(r, \theta)$ of the form

$$C(r, \theta) = r^{\alpha} f(\theta) \tag{39}$$

where the exponent α and the function $f(\theta)$ remain to be determined. Substitution of (39) into the governing Laplace equation $\nabla^2 C = 0$ gives an ordinary differential equation for $f(\theta)$, with solution

$$f(\theta) = A \cos \alpha\theta + B \sin \alpha\theta \tag{40}$$

in terms of the unknowns α, A and B. Now impose the boundary conditions $C(r, \theta = 0) = 0$ and $J_{\theta}(r, \theta = \pi) = 0$ to obtain $A = 0$ and $\cos \pi\alpha = 0$. Of the infinity of eigenvalues for α that satisfy $\cos \pi\alpha = 0$, the choice $\alpha = 1/2$ gives

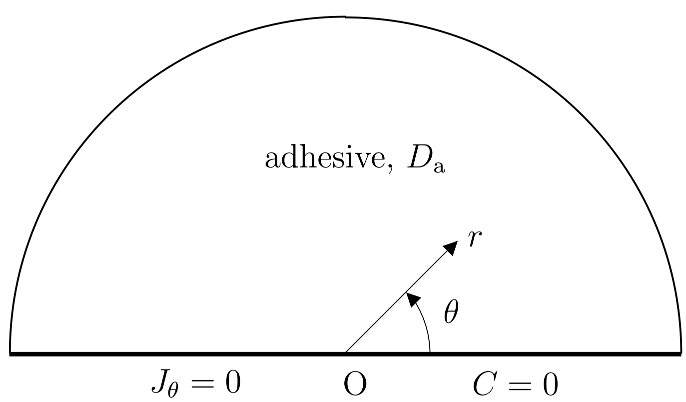

Figure 8: Singularity analysis at the delamination tip leading to the K-field.

the least singular solution in J_i, along with $C(r, \theta = \pi) \to 0$ as $r \to 0$, and implies finite dissipation in a small circular disc encircling the delamination tip. Now re-write B in the form $K = (\pi/2)^{1/2} D_\mathrm{a} B$, such that (39) can be rewritten as

$$C(r, \theta) = \sqrt{\frac{2r}{\pi}} \frac{K}{D_\mathrm{a}} \sin \frac{\theta}{2} \tag{41}$$

along with

$$J_r(r, \theta) = -\frac{K}{\sqrt{2\pi r}} \sin \frac{\theta}{2} \tag{42a}$$

$$J_\theta(r, \theta) = -\frac{K}{\sqrt{2\pi r}} \cos \frac{\theta}{2} \tag{42b}$$

The scalar parameter K is the intensity of the singularity and, analogous to a crack tip in an elastic solid under out-of-plane Mode III loading, K is termed the stress intensity factor (Anderson, 2017). Recall that, in Mode III fracture, analogous expressions to the present diffusion problem hold for the out-of-plane displacement u_z (corresponding to the concentration C), the out-of-plane shear stress τ_{zi} (corresponding to the flux $-J_i$) and the shear modulus μ (corresponding to the diffusion coefficient D_a). Thus, the *K-field* in the present diffusion problem relates to an inverse square root singularity of flux, $J_i \sim 1/\sqrt{r}$. In particular

$$J_n(r) = -J_\theta(r, \theta = 0) = \frac{K}{\sqrt{2\pi r}} \tag{43}$$

In the case where $(h_\mathrm{d}, l) \ll (h_\mathrm{a}, a)$ and $h_\mathrm{d} D_\mathrm{d} \ll h_\mathrm{a} D_\mathrm{a}$, an outer K-field given by (41) exists over an annular domain $(h_\mathrm{d}, l) \ll r \ll (h_\mathrm{a}, a)$. Consequently, all curves in the log-log plot of Fig. 7 converge to a single line of slope $-1/2$, as demanded by (43).

The existence of an outer K-field motivates the following boundary layer problem whereby the remote K-field is applied to a delamination crack of infinite length, $a \to \infty$, in a sandwich layer of infinite height, $h_\mathrm{a} \to \infty$. Accordingly, consider the problem of Fig. 9(a), where an outer K-field is applied via (41). The non-dimensional tip flux, $J_\mathrm{tip}\sqrt{l}/K$, is determined as a function of h_d/l and $D_\mathrm{d}/D_\mathrm{a}$, and the numerical results are given in the form of a contour plot in Fig. 9(b). As anticipated, when the delaminated zone has the same diffusivity as that of the adhesive layer, $D_\mathrm{d} = D_\mathrm{a}$, the tip flux $J_\mathrm{tip}\sqrt{l}/K$ is independent of h_d/l. If $D_\mathrm{d} < D_\mathrm{a}$, $J_\mathrm{tip}\sqrt{l}/K$ decreases with increasing h_d/l, whereas, for the practical case $D_\mathrm{d} > D_\mathrm{a}$, $J_\mathrm{tip}\sqrt{l}/K$ increases with increasing h_d/l.

Additional insight is obtained by re-plotting contours of $J_\mathrm{tip}\sqrt{l}/K$ on a map with axes of h_d/l and the combined non-dimensional group $(h_\mathrm{d}D_\mathrm{d})/(lD_\mathrm{a})$, see Fig. 9(c). Notably, in the practical case $D_\mathrm{d} > D_\mathrm{a}$, the contour lines of $J_\mathrm{tip}\sqrt{l}/K$ have vertical asymptotes for $h_\mathrm{d}/l \to 0$, implying that $J_\mathrm{tip}\sqrt{l}/K$ becomes a function of $(h_\mathrm{d}D_\mathrm{d})/(lD_\mathrm{a})$ only. Asymptotic values of $J_\mathrm{tip}\sqrt{l}/K$ are included in the figure from an additional analysis (given below) of the limit $h_\mathrm{d}/l \to 0$. The limit of $D_\mathrm{d}/D_\mathrm{a} \to 0$ and finite h_d/l is of less practical interest; in this limit $J_\mathrm{tip}\sqrt{l}/K$ is finite and has a value that depends upon h_d/l, see Figs. 9(b) and (c).

Now consider the limit $h_\mathrm{d} \to 0$, with $h_\mathrm{d}D_\mathrm{d}$ remaining finite. Regard the delamination as a strip of infinitesimal height carrying a current $I_\mathrm{d}(x)$, where

$$I_\mathrm{d} = -h_\mathrm{d}D_\mathrm{d}\frac{\partial C}{\partial x} \tag{44}$$

Conservation of mass of the corrodent in the delamination requires

$$\frac{\partial I_\mathrm{d}}{\partial x} = J_n \tag{45}$$

where J_n is the flux from the adhesive into the delamination. Upon recalling

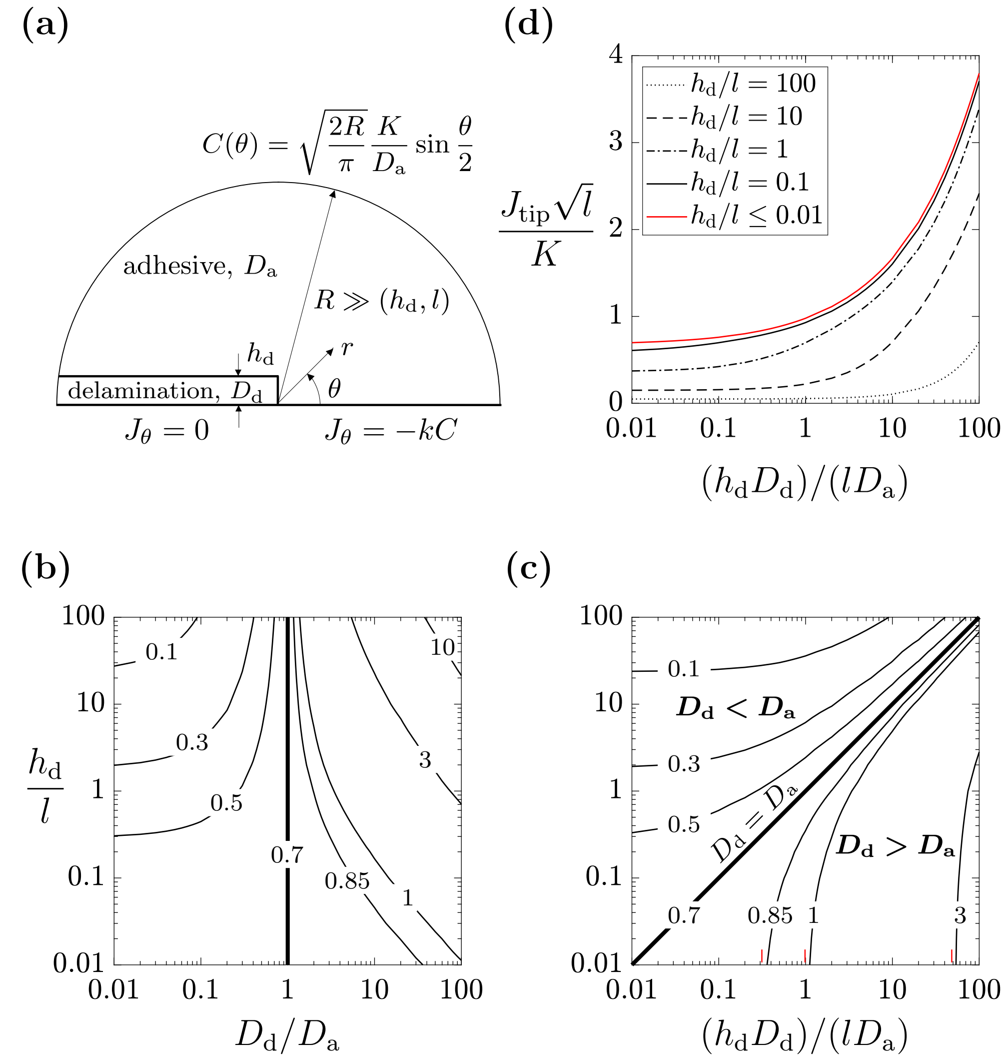

Figure 9: Applied outer K-field: **(a)** boundary layer problem, **(b)** contour plot of $J_{tip}\sqrt{l}/K$ on a map with axes $(D_d/D_a,\ h_d/l)$, **(c)** contour plot of $J_{tip}\sqrt{l}/K$ on a map with axes $((h_d D_d)/(l D_a),\ h_d/l)$, and **(d)** $J_{tip}\sqrt{l}/K$ versus $(h_d D_d)/(l D_a)$ for selected values of h_d/l. As $h_d/l \to 0$, $J_{tip}\sqrt{l}/K$ converges to a limit which is a function of $(h_d D_d)/(l D_a)$ only.

that $J_n = D_{\mathrm{a}}(\partial C/\partial y)$, and making use of (44) and (45), the boundary condition for the diffusion equation $\nabla^2 C = 0$ within the adhesive becomes

$$h_{\mathrm{d}} D_{\mathrm{d}} \frac{\partial^2 C}{\partial x^2} + D_{\mathrm{a}} \frac{\partial C}{\partial y} = 0\,, \qquad x < 0\,,\, y = 0^+ \tag{46}$$

In order to obtain a unique solution with vanishing current at the delamination tip, $I_{\mathrm{d}}(x = 0^-) = 0$, (46) is augmented by the additional condition

$$\left.\frac{\partial C}{\partial x}\right|_{x=0^-} = 0 \tag{47}$$

The boundary layer problem shown in Fig. 9(a) is solved numerically for $h_{\mathrm{d}} = 0$ and by imposing the boundary condition (46) instead of (8). The resulting dependence of $J_{\mathrm{tip}}\sqrt{l}/K$ upon $(h_{\mathrm{d}} D_{\mathrm{d}})/(l D_{\mathrm{a}})$ is plotted in Fig. 9(d) along with predictions for finite values of h_{d}/l, as taken from Fig. 9(c). The limiting value of $J_{\mathrm{tip}}\sqrt{l}/K$ at $h_{\mathrm{d}}/l = 0$ is very close to the numerical results for $h_{\mathrm{d}}/l \leq 0.1$. An analytical expression for a curve fit of $J_{\mathrm{tip}}\sqrt{l}/K$ to $\bar{h} \equiv \log\left[(h_{\mathrm{d}} D_{\mathrm{d}})/(l D_{\mathrm{a}})\right]$ from Fig. 9(d) is:

$$\frac{J_{\mathrm{tip}}\sqrt{l}}{K} \approx 0.991 + 0.349\,\bar{h} + 0.212\,\bar{h}^2 + 0.106\,\bar{h}^3 + 0.0269\,\bar{h}^4 \tag{48}$$

valid over the range $-2 < \bar{h} < 2$.

4.4.1. Calibration of the singularity intensity K

The value of K depends upon geometry and remote boundary conditions. An approximate solution is derived in Appendix A for the asymptotic limit of $a \gg h_{\mathrm{a}}$, by making use of the analogy between the field equations for a Mode III crack in an isotropic linear elastic solid and those for the diffusion problem in steady state. The result (A.6) is repeated here for convenience:

$$K = \frac{\sqrt{2h_{\mathrm{a}}}\, D_{\mathrm{a}} C_0}{a}\,, \qquad a \gg h_{\mathrm{a}} \tag{49}$$

Likewise, an analytic expression for K can be obtained for the other asymptotic limit $a \ll h_\mathrm{a}$. A conformal mapping solution exists for unbounded h_a and is given in Appendix A. The result (A.17) is repeated here:

$$K = \frac{2D_\mathrm{a}C_0}{\sqrt{\pi a}}\,, \qquad a \ll h_\mathrm{a} \tag{50}$$

In Fig. 10, a comparison is given of the asymptotic solutions (49) and (50), along with (48), and the full numerical solution for J_tip. The comparison is given for $(h_\mathrm{d}D_\mathrm{d})/(h_\mathrm{a}D_\mathrm{a}) = 0$ and 0.1, and for $l/h_\mathrm{a} = 0.001$ and 0.01, with the numerical solution making use of the same results as shown in Figs. 3(a) and (b) for the OS regime. As expected, the asymptotic solutions are increasingly accurate as a/h_a departs from 1. Additionally, the asymptotic solution for $a \ll h_\mathrm{a}$ becomes inaccurate as the limit of the ND zone is approached, that

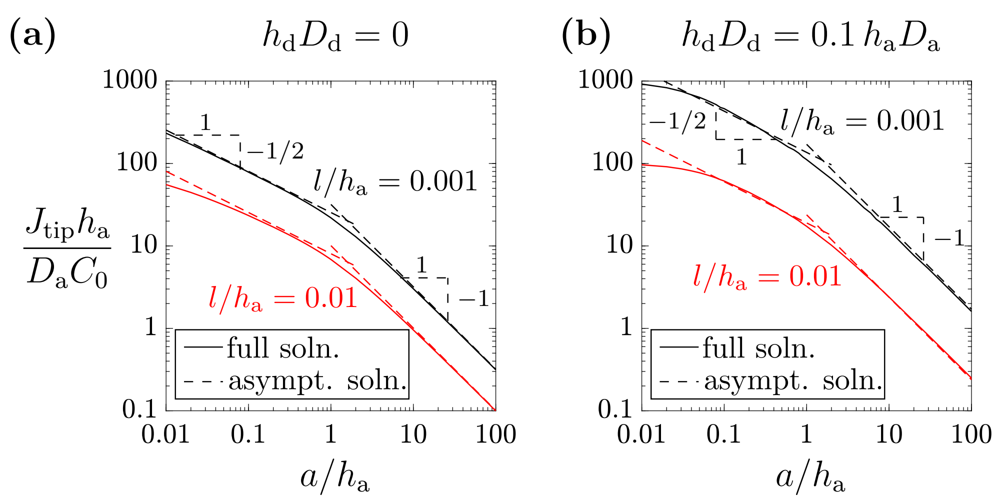

Figure 10: Regime where a unique outer solution (OS) exists. Comparison between full solution and asymptotic solution for $(h_\mathrm{d}D_\mathrm{d})/(h_\mathrm{a}D_\mathrm{a})$ equal to **(a)** 0 and **(b)** 0.1, with l/h_a equal to 0.001 and 0.01. The asymptotic solution is given by (48) and (49) for $a \gg h_\mathrm{a}$, and by (48) and (50) for $a \ll h_\mathrm{a}$.

is, when the value of a approaches the value of l.

5. Singularity analysis at the delamination tip

A singularity analysis for $r \to 0$ is now performed for the case of a finite height h_d of delamination. First, consider the case of $l = 0$, and then the case of $l/h_\mathrm{d} \ll 1$.

5.1. Singularity analysis at the delamination tip for $l = 0$

Proceed to take the limit of an infinitely fast adhesive/metal interface reaction, $k \to \infty$. Then, $l = 0$ and the boundary condition (7) is replaced by $C(r, \theta = 0) = 0$, as shown in Fig. 11. Assume that a separation-of-variables solution again exists for $C(r, \theta)$ in the vicinity of the delamination tip as given by (39). Substitution of (39) into $\nabla^2 C = 0$ in both domains of adhesive and delamination leads to an ordinary differential equation in $f(\theta)$, with solution

$$f(\theta) = A_\mathrm{i} \cos \alpha\theta + B_\mathrm{i} \sin \alpha\theta \tag{51}$$

where A_i and B_i are unknown integration constants, with different values in the adhesive (A_a and B_a) and delamination (A_d and B_d).

The boundary condition $C(r, \theta = 0) = 0$ implies that $A_\mathrm{a} = 0$. The other three integration constants are found by imposing continuity of C and J_θ at the adhesive/delamination interface ($\theta = \pi/2$) and the boundary condition $J_\theta(r, \theta = \pi) = 0$. This results in a homogeneous linear system of three equations that can be written in matrix-vector form as $\underline{\underline{A}} \cdot \underline{X} = \underline{0}$, where $\underline{X} = [A_\mathrm{d}, B_\mathrm{d}, B_\mathrm{a}]^\mathrm{T}$ and $\underline{\underline{A}}$ is the pre-multiplying 3×3 matrix. A non-trivial solution for $\underline{X}$ is obtained by setting $\det \underline{\underline{A}} = 0$, giving rise to the characteristic

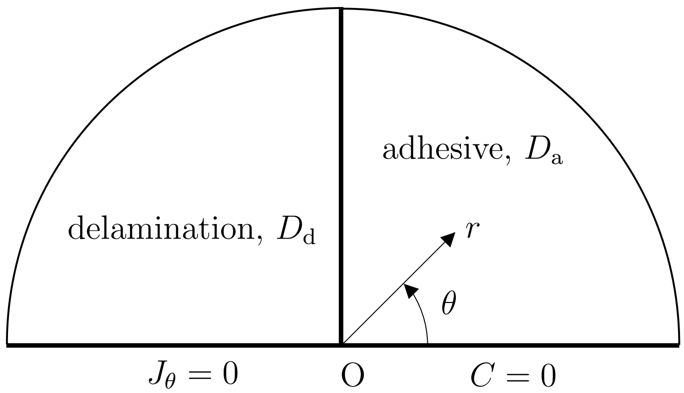

Figure 11: Singularity analysis at the delamination tip.

equation

$$\cos \pi\alpha = \frac{D_d - D_a}{D_d + D_a} \tag{52}$$

Notice that α decreases from 1 to 0 as D_d/D_a increases from 0 to infinity. For each value of α, the constants A_d and B_d can be expressed in terms of B_a.

Upon re-writing B_a in the form $H = (\pi/2)^{1/2} D_a B_a$, the solution for C reads

$$C(r,\theta) = \sqrt{\frac{2}{\pi}} \frac{H}{D_a} r^\alpha \sin \alpha\theta \tag{53}$$

in the adhesive domain $(0 < \theta < \pi/2)$, and

$$C(r,\theta) = \sqrt{\frac{2}{\pi}} \frac{H}{D_a} r^\alpha \left[\cos \pi\alpha \tan(\pi\alpha/2) \cos \alpha\theta + (1 - \cos \pi\alpha) \sin \alpha\theta\right] \tag{54}$$

in the delamination domain $(\pi/2 < \theta < \pi)$. It is emphasised that the value of α is given by (52), for any assumed value of D_d/D_a. The radial and circumferential fluxes follow immediately from $\boldsymbol{J}_i = -D_i \boldsymbol{\nabla} C$ as

$$J_r(r,\theta) = -\sqrt{\frac{2}{\pi}} \alpha H r^{\alpha-1} \sin \alpha\theta \tag{55a}$$

$$J_\theta(r,\theta) = -\sqrt{\frac{2}{\pi}}\alpha H r^{\alpha-1}\cos\alpha\theta \tag{55b}$$

in the adhesive domain, and

$$J_r(r,\theta) = -\sqrt{\frac{2}{\pi}}\frac{D_\mathrm{d}}{D_\mathrm{a}}\alpha H r^{\alpha-1}\left[\cos\pi\alpha\tan(\pi\alpha/2)\cos\alpha\theta + (1-\cos\pi\alpha)\sin\alpha\theta\right] \tag{56a}$$

$$J_\theta(r,\theta) = -\sqrt{\frac{2}{\pi}}\frac{D_\mathrm{d}}{D_\mathrm{a}}\alpha H r^{\alpha-1}\left[-\cos\pi\alpha\tan(\pi\alpha/2)\sin\alpha\theta + (1-\cos\pi\alpha)\cos\alpha\theta\right] \tag{56b}$$

in the delamination domain. Equations (53)-(56) define the so-called H*-field*, which is valid as $r \to 0$. In particular, the normal flux at the adhesive/metal interface ($\theta = 0$) reads

$$J_n(r) = -J_\theta(r,\theta=0) = \sqrt{\frac{2}{\pi}}\alpha H r^{\alpha-1} \tag{57}$$

For illustrative purposes, now consider the three choices $D_\mathrm{d}/D_\mathrm{a} = 0$, 1 and ∞.

Case (i): $D_\mathrm{d}/D_\mathrm{a} = 0$. Zero corrodent is transported along the delamination, and $\alpha = 1$ from (52). The asymptotic solution in the adhesive is

$$C(r,\theta) = \sqrt{\frac{2}{\pi}}\frac{H}{D_\mathrm{a}} r\sin\theta = \sqrt{\frac{2}{\pi}}\frac{H}{D_\mathrm{a}} y \tag{58a}$$

$$J_r(r,\theta) = -\sqrt{\frac{2}{\pi}} H\sin\theta \tag{58b}$$

$$J_\theta(r,\theta) = -\sqrt{\frac{2}{\pi}} H\cos\theta \tag{58c}$$

and consequently

$$J_n(r) = -J_\theta(r,\theta=0) = \sqrt{\frac{2}{\pi}} H \tag{59}$$

This solution has a straightforward interpretation in Cartesian co-ordinates (x, y): the flux directly ahead of the delamination tip is uniform, independent of r, such that $J_x = 0$ and $J_y = -\sqrt{2}H/\sqrt{\pi}$.

Case (ii): $D_\mathrm{d}/D_\mathrm{a} = 1$. The diffusion domain comprises the adhesive only, as sketched in Fig. 8, and $\alpha = 1/2$ from (52). Upon rephrasing H as the "stress intensity factor" K, the so-called K-*field* given by (41) and (42) is recovered. The flux ahead of the delamination tip is given by (43) and is characterised by an inverse square root singularity, $J_n \sim Kr^{-1/2}$.

Case (iii): $D_\mathrm{d}/D_\mathrm{a} \to \infty$. Transport along the delamination is so fast that $C = C_0$ therein, and $\alpha \to 0$ via (52). The asymptotic solution in the adhesive is

$$C(\theta) = \frac{2}{\pi} C_0 \theta \tag{60a}$$

$$J_r = 0\,, \tag{60b}$$

$$J_\theta(r) = -\frac{D_\mathrm{a}}{r}\frac{2}{\pi} C_0 \tag{60c}$$

implying that

$$J_n(r) = -J_\theta(r) = \frac{D_\mathrm{a}}{r}\frac{2}{\pi} C_0 \tag{61}$$

Thus, the flux ahead of the delamination tip is characterised by an inverse singularity, $J_n \sim D_\mathrm{a} C_0 r^{-1}$. This solution resembles a *dislocation field*, in view of the close analogy to the out-of-plane displacement field for a screw dislocation in an elastic solid (Hull and Bacon, 2011).

5.2. Embedded singularity

The H-field as given by (53) and (54) exists in the limit $r \to 0$, for every value of $D_\mathrm{d}/D_\mathrm{a}$, with α given by (52). Additionally, if $h_\mathrm{d} D_\mathrm{d}$ is much less than $h_\mathrm{a} D_\mathrm{a}$, then a so-called "outer K-field" of the form (41) exists over an outer domain, $h_{\mathrm{d}} \ll r \ll (h_{\mathrm{a}}, a)$; the inner H-field is embedded within the outer K-field, as sketched in Fig. 12. A transition zone exists between the inner zone (H-field) and the outer zone (K-field). This is an example of an *embedded singularity*, and is reminiscent of the small-scale yielding problem in elastic-plastic fracture mechanics, whereby an asymptotic near tip HRR plastic field (Hutchinson, 1968; Rice and Rosengren, 1968) is embedded within an outer K-dominated zone. In contrast, when $h_{\mathrm{d}}D_{\mathrm{d}}$ is not much less than $h_{\mathrm{a}}D_{\mathrm{a}}$, the outer K-field vanishes, but an inner H-field still exists as $r \to 0$. This is analogous to the elastic-plastic case in standard fracture mechanics, where the presence of a large plastic zone ahead of the crack tip eliminates

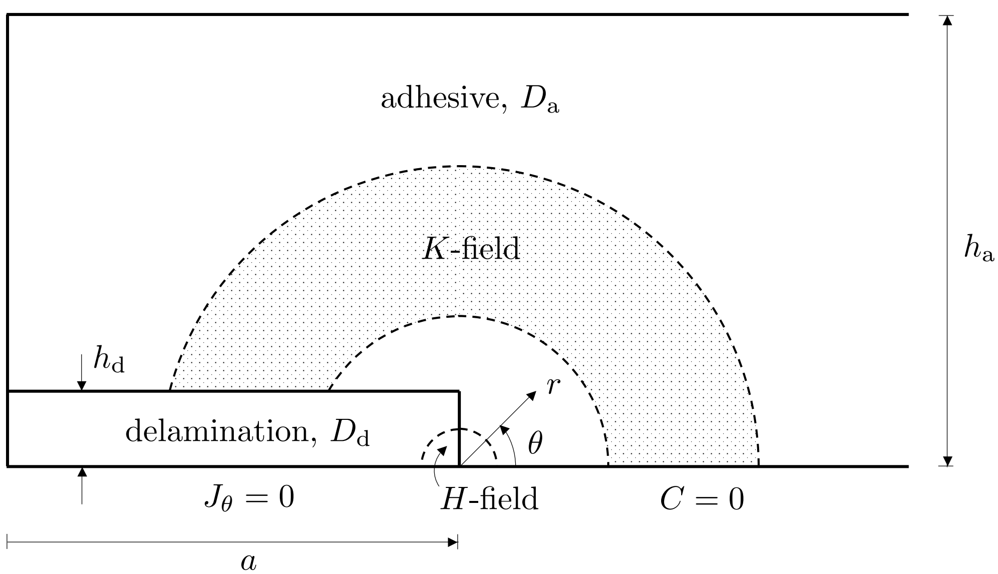

Figure 12: H-field embedded in K-field.

the outer K-field, but the near tip J-field still exists (Anderson, 2017).[2] Embedded singularities are pervasive in fracture mechanics; for example, they also arise in the fracture of a sandwich layer (Fleck et al., 1991; Akisanya and Fleck, 1997) and in the detachment of an adhered micropillar from a dissimilar substrate (Khaderi et al., 2015).

Now focus on the case of an embedded singularity, such that an outer K-field (41) exists in the current diffusion problem. Recall that, for the case $l = 0$,

(i) Concentrations and fluxes scale linearly with the value of K, see (41) and (42);

(ii) The only geometrical length scale entering the problem is $h_{\rm d}$; and

(iii) The solution depends upon the value of the ratio $D_{\rm d}/D_{\rm a}$.

Dimensional analysis and linearity require that H and K are related through

$$H = K h_{\rm d}^{\frac{1-2\alpha}{2}} g_1 \tag{62}$$

where the calibration function g_1 depends only upon $D_{\rm d}/D_{\rm a}$, and can be determined as follows.

For each assumed value of $D_{\rm d}/D_{\rm a}$, the corresponding value of α is given by (52). Next, solve the boundary layer problem for Laplace's equation (10), by imposing the outer K-field (41) on the outermost boundary of the mesh, and by choosing a convenient value of K, see Fig. 13(a). Substitution of (62)

[2] It is emphasised that here J denotes a path-independent line integral in fracture mechanics and not diffusion flux.

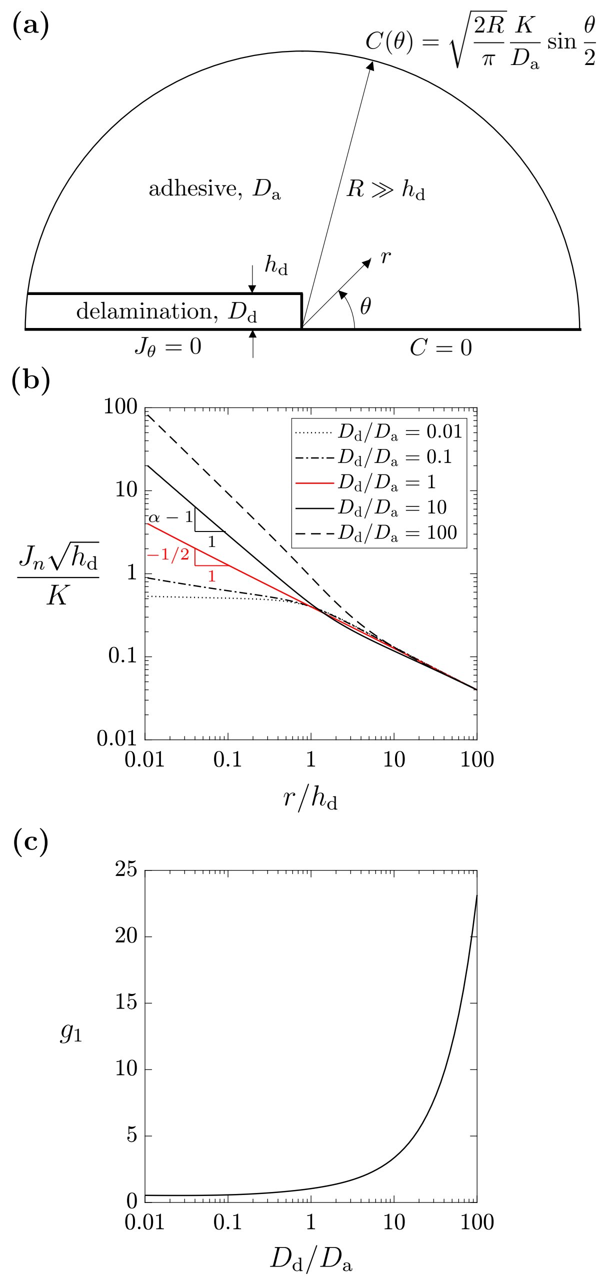

Figure 13: **(a)** Boundary layer problem for the case $l = 0$, where the outer K-field is applied to the periphery of the idealised specimen; **(b)** interfacial flux distribution J_n directly ahead of the delamination tip; **(c)** calibration function $g_1(D_\mathrm{d}/D_\mathrm{a})$.

into (57) reveals that, as $r \to 0$,

$$\frac{J_n\sqrt{h_\mathrm{d}}}{K} = \sqrt{\frac{2}{\pi}}\left(\frac{r}{h_\mathrm{d}}\right)^{\alpha-1}\alpha g_1 \tag{63}$$

A series of numerical simulations has been performed for selected values of $D_\mathrm{d}/D_\mathrm{a}$, see Fig. 13(b), and each displays the asymptotic response (63) as $r \to 0$. A best fit to the plot of $\log\left(J_n\sqrt{h_\mathrm{d}}/K\right)$ versus $\log\left(r/h_\mathrm{d}\right)$ over the range $-2 < \log\left(r/h_\mathrm{d}\right) < -0.5$ is used to determine the value of g_1, and the resulting dependence of g_1 upon $D_\mathrm{d}/D_\mathrm{a}$ is plotted in Fig. 13(c). For the special case $D_\mathrm{d}/D_\mathrm{a} = 1$, it follows that $\alpha = 1/2$, $g_1 = 1$ and (63) reduces to (43).

Finally, consider the case where $l \ll h_\mathrm{d}$, but remains finite. An inner H-field exists for $l \ll r \ll h_\mathrm{d}$. Recall:

(i) Concentrations and fluxes scale linearly with the value of H, see (53)-(56);

(ii) The dominant geometrical length scale entering the problem is l; and

(iii) The solution depends upon the value of the ratio $D_\mathrm{d}/D_\mathrm{a}$.

Dimensional analysis and linearity require that J_tip and H are related through

$$J_\mathrm{tip} = H l^{\alpha-1} g_2 \tag{64}$$

where g_2 is a function of $D_\mathrm{d}/D_\mathrm{a}$ to be found. If an outermost K-field embeds the inner H-field, then, upon substituting (62) into (64), the coupling relation between J_tip and K is of the form

$$\frac{J_\mathrm{tip}\sqrt{l}}{K} = \left(\frac{h_\mathrm{d}}{l}\right)^{\frac{1-2\alpha}{2}} g_1\, g_2\,, \qquad h_\mathrm{d} \gg l \tag{65}$$

The predicted dependence of $J_{\rm tip}$ upon K is verified by a series of numerical simulations for selected values of $D_{\rm d}/D_{\rm a}$, see Fig. 14(a). Each curve displays the expected asymptotic response (65), that is, $\log\left(J_{\rm tip}\sqrt{l}/K\right)$ is linear with $\log\left(h_{\rm d}/l\right)$ for $h_{\rm d} \gg l$. Note that, for the special case $D_{\rm d} = D_{\rm a}$, the exponent α equals $1/2$ and $J_{\rm tip}$ is insensitive to $h_{\rm d}/l$. For $D_{\rm d} < D_{\rm a}$, α exceeds $1/2$ and $J_{\rm tip}$ decreases with increasing $h_{\rm d}/l$; conversely, for $D_{\rm d} > D_{\rm a}$, α is less than $1/2$ and $J_{\rm tip}$ increases with increasing $h_{\rm d}/l$. Since g_1 is already known (see Fig. 13(c)), a best fit to the plot of $\log\left(J_{\rm tip}\sqrt{l}/K\right)$ versus $\log\left(h_{\rm d}/l\right)$ over the range $1 < \log\left(h_{\rm d}/l\right) < 2$ is used to determine the value of g_2, and the resulting dependence of g_2 upon $D_{\rm d}/D_{\rm a}$ is plotted in Fig. 14(b).

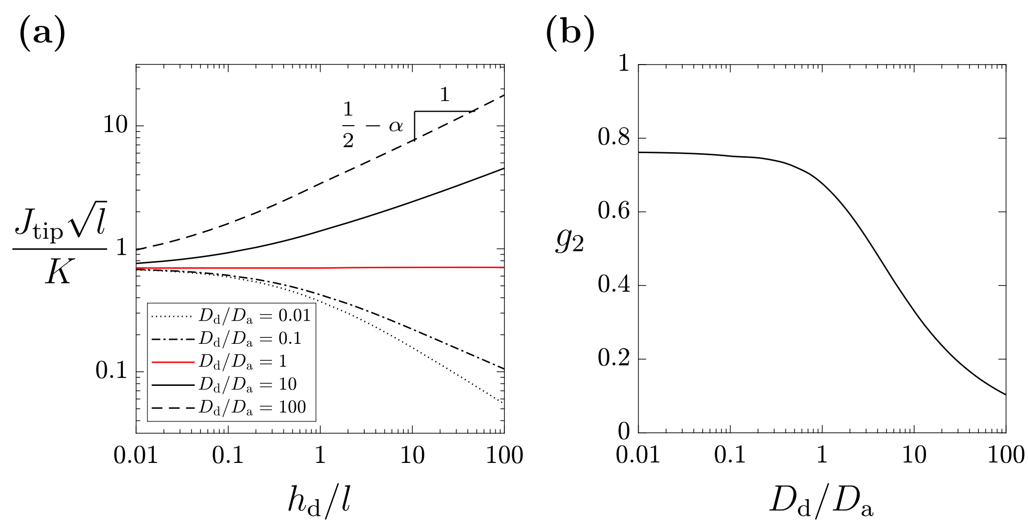

Figure 14: **(a)** Interfacial flux at delamination tip $J_{\rm tip}$ for the case of a finite value of l; **(b)** calibration function $g_2(D_{\rm d}/D_{\rm a})$.

6. Discussion: accuracy of the steady-state assumption

Recall that an initial transient, of duration t_I, is required to establish a steady-state flux J_tip. Contour plots of $t_\mathrm{I} D_\mathrm{a}/h_\mathrm{a}^2$ as a function of a/h_a and l/h_a are shown in Fig. 15 for four selected values of $(h_\mathrm{d} D_\mathrm{d})/(h_\mathrm{a} D_\mathrm{a})$. These plots are obtained by numerically solving the time-dependent diffusion equation (6), with the duration of the initial transient t_I already defined in (11). Attention is again restricted to the case where h_d is much smaller than all other length scales entering the problem. The value of $t_\mathrm{I} D_\mathrm{a}/h_\mathrm{a}^2$ increases with increasing a/h_a and l/h_a and with decreasing $(h_\mathrm{d} D_\mathrm{d})/(h_\mathrm{a} D_\mathrm{a})$. The dependence of $t_\mathrm{I} D_\mathrm{a}/h_\mathrm{a}^2$ upon a/h_a, l/h_a and $(h_\mathrm{d} D_\mathrm{d})/(h_\mathrm{a} D_\mathrm{a})$ contrasts with that of $J_\mathrm{tip} h_\mathrm{a}/(D_\mathrm{a} C_0)$, compare Figs. 3 and 15. For example, the contours of $J_\mathrm{tip} h_\mathrm{a}/(D_\mathrm{a} C_0)$ are approximately horizontal (especially for large values of $(h_\mathrm{d} D_\mathrm{d})/(h_\mathrm{a} D_\mathrm{a})$ and for small values of a/h_a), whereas those of $t_\mathrm{I} D_\mathrm{a}/h_\mathrm{a}^2$ are approximately vertical (especially for large values of $(h_\mathrm{d} D_\mathrm{d})/(h_\mathrm{a} D_\mathrm{a})$ and for small values of l/h_a). Rephrased, $J_\mathrm{tip} h_\mathrm{a}/(D_\mathrm{a} C_0)$ is mainly affected by l/h_a, whereas $t_\mathrm{I} D_\mathrm{a}/h_\mathrm{a}^2$ is mainly affected by a/h_a. The value of $(h_\mathrm{d} D_\mathrm{d})/(h_\mathrm{a} D_\mathrm{a})$ has a significant effect upon both $J_\mathrm{tip} h_\mathrm{a}/(D_\mathrm{a} C_0)$ and $t_\mathrm{I} D_\mathrm{a}/h_\mathrm{a}^2$.

During the initial transient phase, of duration t_I, the interfacial flux at the delamination tip increases progressively until it attains the steady-state value J_tip. The quantity of corrodent per unit area of interface Q_I that has reacted at the delamination tip during the transient phase according to (12) is a small fraction of $J_\mathrm{tip}\, t_\mathrm{I}$. Consequently, if the amount of reacted corrodent (per unit area) to disbond the interface Q^* satisfies, or exceeds, the value

$$Q^*_\mathrm{min} = J_\mathrm{tip}\, t_\mathrm{I} \tag{66}$$

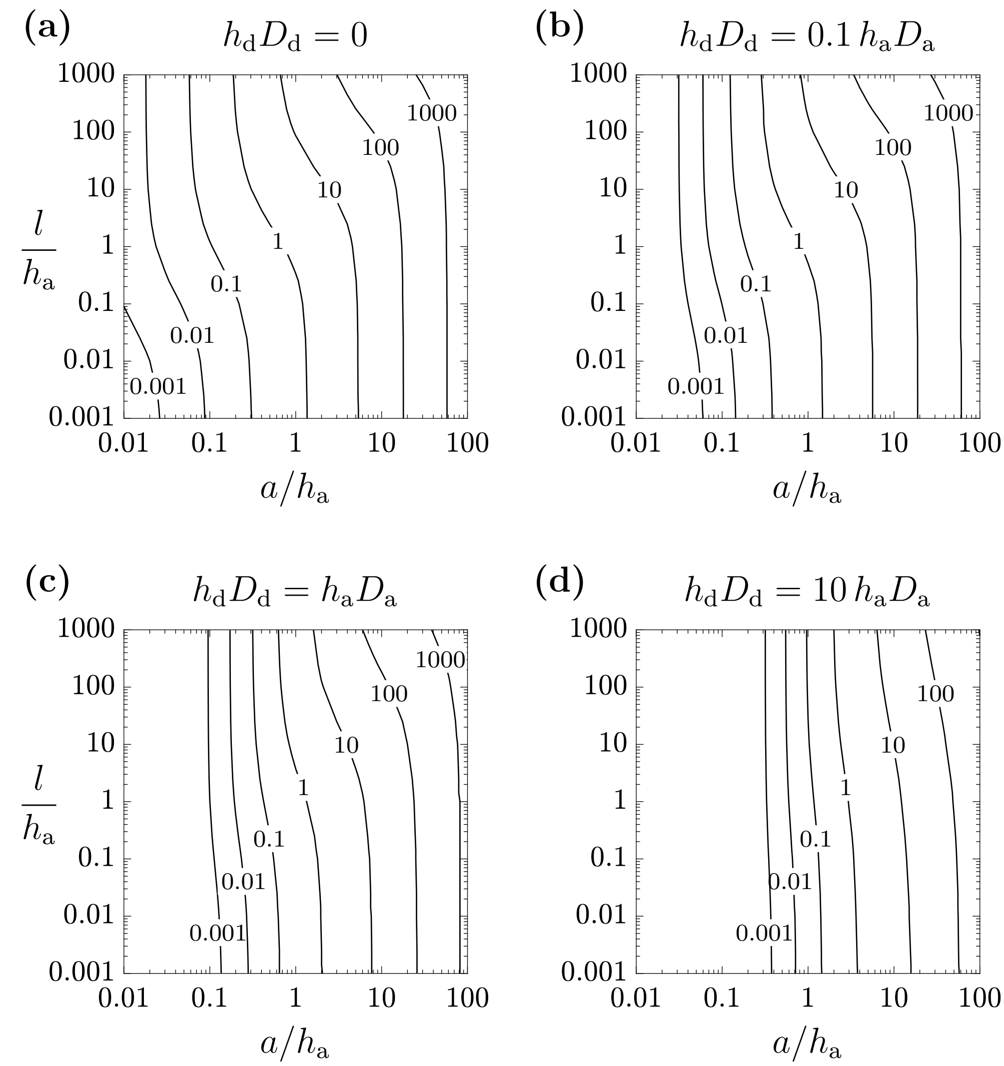

Figure 15: Contour plots of $t_I D_a/h_a^2$ on a map with axes (a/h_a, l/h_a), for $(h_d D_d)/(h_a D_a)$ equal to **(a)** 0, **(b)** 0.1, **(c)** 1 and **(d)** 10.

then the corresponding delamination time is dictated by the steady-state solution according to (16). Thus, $Q^*_{\rm min}$ can be taken as the critical amount of reacted corrodent that is required in order to neglect the transient phase.

Contour plots of $Q^*_{\rm min}/(C_0 h_{\rm a})$ as a function of $a/h_{\rm a}$ and $l/h_{\rm a}$ are given in Fig. 16 for selected values of $(h_{\rm d} D_{\rm d})/(h_{\rm a} D_{\rm a})$. These plots are obtained by combining the values of $J_{\rm tip} h_{\rm a}/(D_{\rm a} C_0)$ and $t_{\rm I} D_{\rm a}/h_{\rm a}^2$ in Figs. 3 and 15 via (66). The value of $Q^*_{\rm min}/(C_0 h_{\rm a})$ is largely dictated by the value of a/l, with only mild sensitivity to $(h_{\rm d} D_{\rm d})/(h_{\rm a} D_{\rm a})$. At large a/l (bottom-right corner of the maps in Fig. 16), $Q^*_{\rm min}/(C_0 h_{\rm a})$ is large and the delamination time is likely to be dictated by the initial transient. In contrast, at small a/l (top-left corner of the maps), $Q^*_{\rm min}/(C_0 h_{\rm a})$ is small and delamination growth is likely to initiate long after steady state has been attained.

7. Concluding remarks

The diffusion of a corrodent in a pre-cracked adhesive layer from an infinite reservoir to the adhesive/substrate interface has been addressed. It has been assumed that interfacial crack growth begins when the total amount of corrodent that has reacted ahead of the crack tip attains a critical value.

Four regimes of behaviour, corresponding to different asymptotic limits of the non-dimensional groups entering the problem, have been identified for the case where the debonding time much exceeds the duration of the initial transient. The steady-state flux of corrodent to the adhesive/substrate interface ahead of the crack tip, $J_{\rm tip}$, has been quantified for all regimes, and the results show good agreement with the full numerical solution.

One of the four regimes is characterised by an outer singular field of flux,

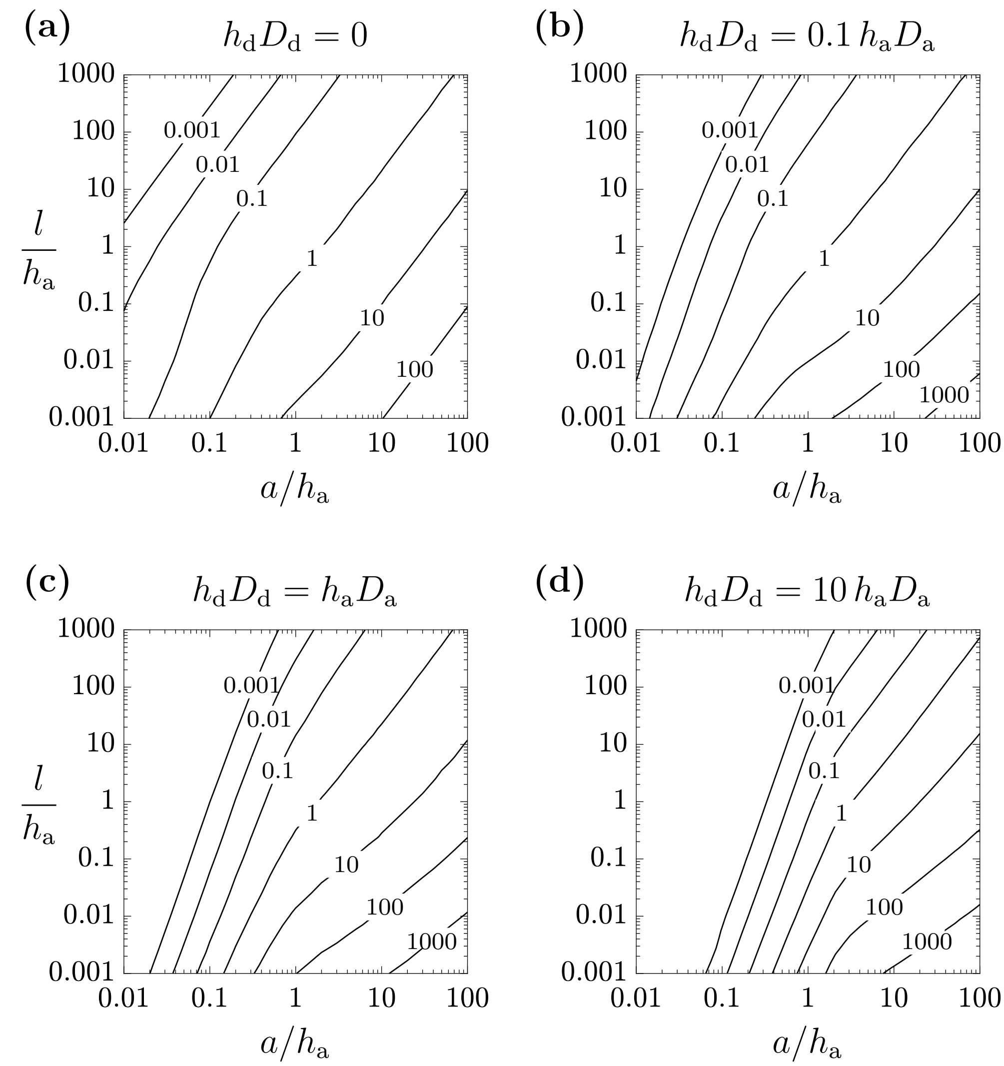

Figure 16: Contour plots of $Q^*_{\min}/(C_0\, h_a)$ on a map with axes $(a/h_a,\ l/h_a)$, for $(h_d D_d)/(h_a D_a)$ equal to **(a)** 0, **(b)** 0.1, **(c)** 1 and **(d)** 10.

of intensity K, that surrounds the crack tip, analogous to the Mode III K-field of linear elastic fracture mechanics. The tip flux can be found by imposing the K-field remotely from the crack tip, and by relating K to the geometry of the specimen. A singularity analysis of the inner field has been given for the flux in the vicinity of the delamination tip in the limit of an infinitely fast interface reaction, implying $l = 0$. The coupling coefficients between the inner and outer singular fields have been obtained, and the difference in exponent of spatial dependence of the singularities demands that the coupling relations involve the height h_{d} of the delamination.

This study quantifies the time for the initiation of delamination growth in a sandwich layer by diffusion of a corrosive species, and lays the groundwork for a future study on the rate of delamination growth.

Acknowledgements

The authors are grateful for financial support from the ERC advanced research grant MULTILAT. Also, this project has received funding from the Interreg 2 Seas programme 2014-2020 co-funded by the European Regional Development Fund under subsidy contract No 03-051. The authors are grateful to Prof. Vikram Deshpande and to Dr. Sina Askarinejad for insightful discussions.

Appendix A. Calibration of K

Appendix A.1. The case $a \gg h_a$. Solution by analogy with a Mode III crack.

An analytic solution is obtained for K in the limit $a \gg h_{\mathrm{a}}$ by considering the analogous Mode III elasticity problem sketched in Fig. A.17. Write u_z as

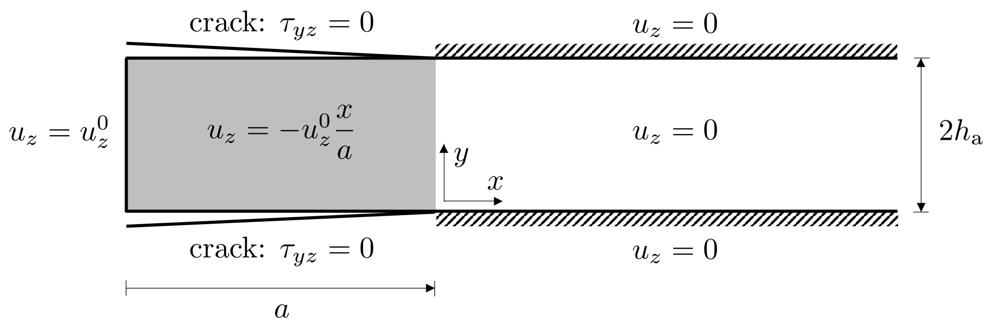

Figure A.17: Evaluation of K for $a \gg h_\mathrm{a}$ in an elastic solid under Mode III loading by making use of the energy release rate. Strain energy is stored in the grey zone ($x < a$).

the out-of-plane displacement, $\gamma_{zi} = \partial u_z / \partial x_i$ as the shear strain, τ_{zi} as the shear stress and μ as the shear modulus in the Mode III elasticity problem. Recall that an analogy has already been made in Sec. 4.4 between the Mode III elastic fracture problem and the steady-state diffusion problem such that

$$u_z \leftrightarrow C\,, \qquad \gamma_{zi} \leftrightarrow \frac{\partial C}{\partial x_i}\,, \qquad \tau_{zi} \leftrightarrow -J_i\,, \qquad \mu \leftrightarrow D_\mathrm{a} \tag{A.1}$$

The strain energy W stored in a strip of adhesive of height $2h_\mathrm{a}$ and subjected to an imposed displacement u_z^0 at its left-hand side is approximately

$$W \approx \frac{1}{2}\mu \left(\frac{u_z^0}{a}\right)^2 2h_\mathrm{a} a \tag{A.2}$$

The adhesive strip in the side-clamped region $x > a$ provides a negligible contribution to W. The energy release rate G associated with crack advance reads (Rice, 1968)

$$G = -\frac{1}{2}\frac{\partial W}{\partial a}\bigg|_{u_z^0} = \frac{1}{2}\mu h_\mathrm{a} \left(\frac{u_z^0}{a}\right)^2 \tag{A.3}$$

where the factor $1/2$ is due to the presence of two cracks in the geometry shown in Fig. A.17. Recall that, for Mode III fracture of an interfacial crack between an elastic solid of shear modulus μ and a rigid substrate, G is related to K via[3]

$$G = \frac{K^2}{4\mu} \tag{A.4}$$

Now substitute (A.3) into (A.4), to obtain

$$K = \frac{\sqrt{2h_{\mathrm{a}}}\,\mu\, u_z^0}{a} \tag{A.5}$$

and convert this into the analogous expression for the diffusion problem,

$$K = \frac{\sqrt{2h_{\mathrm{a}}} D_{\mathrm{a}} C_0}{a} \tag{A.6}$$

Appendix A.2. The case $a \ll h_a$. Solution through conformal mapping.

If $a \ll h_{\mathrm{a}}$ (and $l = 0$), the only length scale in the problem is the delamination length a. Introduce a new co-ordinate $X = x + a$, such that the origin shifts from the delamination tip to the left-hand free-face of the adhesive layer. Extend the quarter-plane problem in the physical plane (x, y) into a full-plane problem in the complex plane $z = X + iy$, where $i = \sqrt{-1}$ denotes the imaginary number, as shown in Fig. A.18. Since $C(X, y)$ satisfies Laplace's equation, a complex function $\Phi(z)$ exists, with real part equal to $C(X, y)$, such that

$$\Phi(z) = C(X, y) + i\Psi(X, y) \tag{A.7}$$

The complementary function $\Psi(X, y)$ also satisfies Laplace's equation, and can be obtained from $C(X, y)$ via the Cauchy-Riemann equations, if necessary. It plays the role of a stream function.

[3]The value of G in (A.4) equals a half of the value of G for a Mode III crack *within* an elastic solid (Anderson, 2017).

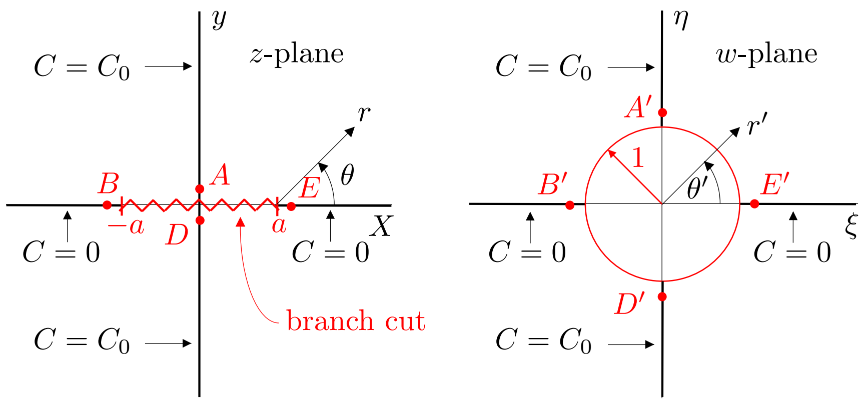

Figure A.18: Conformal mapping of the problem in the complex plane $z = X + iy$ into the complex plane $w = \xi + i\eta$ by the mapping function $2z/a = w + (1/w)$.

In order to obtain $\Phi(z)$, it is convenient to use a conformal mapping technique (Hildebrand, 1976) and map the z-plane into a complex plane $w = \xi + i\eta$ (see Fig. A.18), by employing the mapping function

$$\frac{z}{a} = \frac{1}{2}\left(w + \frac{1}{w}\right) \tag{A.8}$$

with inverse

$$w = \frac{z}{a} + \sqrt{\left(\frac{z}{a}\right)^2 - 1} \tag{A.9}$$

The line segment $(|x| \leq a, y = 0)$ in the z-plane contains a branch cut that maps onto the unit circle of the w-plane. Selected points $ABDE$ in the z-plane have images $A'B'D'E'$ in the w-plane, as shown in Fig. A.18: the relevant branch of the mapping function $w(z)$ is the domain exterior to the unit circle of the w-plane.

It is straightforward to obtain the solution for Φ in the mapped plane w.

Assume that the solution is

$$\Phi(w) = -i\frac{2}{\pi}C_0 \ln w \tag{A.10}$$

Now introduce polar co-ordinates (r', θ') in the w-plane (see Fig. A.18), such that $w = r' \exp(i\theta')$. Equation (A.10) becomes

$$\Phi = \frac{2}{\pi}C_0\theta' - i\frac{2}{\pi}C_0 \ln r' \tag{A.11}$$

and

$$C = \mathrm{Re}(\Phi) = \frac{2}{\pi}C_0\theta' \tag{A.12}$$

This solution satisfies the required boundary conditions of the physical problem: $C(\theta' = 0) = 0$ and $C(\theta' = \pi/2) = C_0$. Upon making use of (A.9), the solution (A.10) in the z-plane is

$$\Phi(z) = -i\frac{2}{\pi}C_0 \ln\left(\frac{z}{a} + \sqrt{\left(\frac{z}{a}\right)^2 - 1}\right) \tag{A.13}$$

Now write

$$z = X + iy = a + r\exp(i\theta) \tag{A.14}$$

where r and θ are the polar co-ordinates with origin at $z = a$ (see Fig. A.18). In order to evaluate K, restrict attention to $r \ll a$; then, (A.13) has the asymptotic form

$$\Phi(z) \approx -i\frac{2}{\pi}C_0\sqrt{\frac{2r}{a}}\exp\left(i\frac{\theta}{2}\right) = \frac{2}{\pi}C_0\sqrt{\frac{2r}{a}}\left(\sin\frac{\theta}{2} - i\cos\frac{\theta}{2}\right) \tag{A.15}$$

and consequently

$$C = \mathrm{Re}[\Phi(z)] \approx \frac{2}{\pi}C_0\sqrt{\frac{2r}{a}}\sin\frac{\theta}{2} \qquad \text{as } r \to 0 \tag{A.16}$$

Upon matching the K-field (41) to (A.16), the value of K follows immediately as

$$K = \frac{2D_{\mathrm{a}}C_0}{\sqrt{\pi a}} \tag{A.17}$$

References

Akisanya, A.R., Fleck, N.A., 1997. Interfacial cracking from the freeedge of a long bi-material strip. International Journal of Solids and Structures 34, 1645–1665.

Anderson, T.L., 2017. Fracture Mechanics: Fundamentals and Applications. CRC Press, Boca Raton, FL (USA).

Bordes, M., Davies, P., Cognard, J.Y., Sohier, L., Sauvant-Moynot, V., Galy, J., 2009. Prediction of long term strength of adhesively bonded steel/epoxy joints in sea water. International Journal of Adhesion and Adhesives 29, 595–608. Special Issue on Durability of Adhesive Joints.

Carslaw, H.S., Jaeger, J.C., 1959. Conduction of Heat in Solids. Oxford University Press, Oxford, UK.

Fleck, N.A., Hutchinson, J.W., Suo, Z., 1991. Crack path selection in a brittle adhesive layer. International Journal of Solids and Structures 27, 1683–1703.

Fleck, N.A., Willis, J.R., 2021. Steady-state growth of an interfacial crack by corrosion. Journal of the Mechanics and Physics of Solids 148, 104268.

Gettings, M., Baker, F.S., Kinloch, A.J., 1977. Use of auger and x-ray photoelectron spectroscopy to study the locus of failure of structural adhesive joints. Journal of Applied Polymer Science 21, 2375–2392.

Gledhill, R.A., Kinloch, A.J., 1974. Environmental failure of structural adhesive joints. The Journal of Adhesion 6, 315–330.

Hildebrand, F.B., 1976. Advanced Calculus for Applications. 2nd ed., Prentice Hall, Hoboken, NJ (USA).

Hull, D., Bacon, D.J., 2011. Introduction to Dislocations. Elsevier, Oxford, UK.

Hutchinson, J.W., 1968. Singular behaviour at the end of a tensile crack in a hardening material. Journal of the Mechanics and Physics of Solids 16, 13–31.

Khaderi, S.N., Fleck, N.A., Arzt, E., McMeeking, R.M., 2015. Detachment of an adhered micropillar from a dissimilar substrate. Journal of the Mechanics and Physics of Solids 75, 159–183.

Kinloch, A.J., 1979. Interfacial fracture mechanical aspects of adhesive bonded joints-A review. The Journal of Adhesion 10, 193–219.

Leidheiser, H., 1987. Cathodic delamination of polybutadiene from steel-A review. Journal of Adhesion Science and Technology 1, 79–98.

Leng, A., Streckel, H., Hofmann, K., Stratmann, M., 1998a. The delamination of polymeric coatings from steel. Part 3: Effect of the oxygen partial pressure on the delamination reaction and current distribution at the metal/polymer interface. Corrosion Science 41, 599–620.

Leng, A., Streckel, H., Stratmann, M., 1998b. The delamination of polymeric coatings from steel. Part 1: Calibration of the Kelvinprobe and basic delamination mechanism. Corrosion Science 41, 547–578.

Merah, N., Nizamuddin, S., Khan, Z., Al-Sulaiman, F., Mehdi, M., 2010. Effects of harsh weather and seawater on glass fiber reinforced epoxy composite. Journal of Reinforced Plastics and Composites 29, 3104–3110.

Poursaee, A. (Ed.), 2016. Corrosion of Steel in Concrete Structures. Woodhead Publishing, Oxford, UK.

Rice, J.R., 1968. A path independent integral and the approximate analysis of strain concentration by notches and cracks. Journal of Applied Mechanics 35, 379–386.

Rice, J.R., Rosengren, G.F., 1968. Plane strain deformation near a crack tip in a power-law hardening material. Journal of the Mechanics and Physics of Solids 16, 1–12.

Schmidt, R.G., Bell, J.P., 1986. Epoxy adhesion to metals, in: Dušek, K. (Ed.), Epoxy Resins and Composites II, Springer Berlin Heidelberg. pp. 33–71.

Stratmann, M., Feser, R., Leng, A., 1994. Corrosion protection by organic films. Electrochimica Acta 39, 1207–1214.